



WEST UNIVERSITY OF TIMIȘOARA
FACULTY OF MATHEMATICS AND COMPUTER
SCIENCE

MASTER STUDY PROGRAM:
Artificial Intelligence and Distributed Computing

MASTER THESIS

SUPERVISOR:
Lect. Dr. Marian Neagul

GRADUATE:
Alexandru-Constantin Munteanu

TIMIȘOARA
2021

WEST UNIVERSITY OF TIMIȘOARA
FACULTY OF MATHEMATICS AND COMPUTER
SCIENCE
MASTER STUDY PROGRAM:
Artificial Intelligence and Distributed Computing

Semantic Segmentation of Vegetation in Remote Sensing Imagery Using Deep Learning

SUPERVISOR:
Lect. Dr. Marian Neagul

GRADUATE:
Alexandru-Constantin Munteanu

TIMIȘOARA
2021

Abstract

In recent years, the geospatial industry has been developing at a steady pace. This growth implies the addition of satellite constellations that produce a copious supply of satellite imagery and other Remote Sensing data on a daily basis. Sometimes, this information, even if in some cases we are referring to publicly available data, it sits unaccounted for due to the sheer size of it. Processing such large amounts of data with the help of human labour or by using traditional automation methods is not always a viable solution from the standpoint of both time and other resources.

Within the present work, we propose an approach for creating a multi-modal and spatio-temporal dataset comprised of publicly available Remote Sensing data and testing for feasibility using state of the art Machine Learning (ML) techniques. Precisely, the usage of Convolutional Neural Networks (CNN) models that are capable of separating different classes of vegetation that are present in the proposed dataset. Popularity and success of similar methods in the context of Geographical Information Systems (GIS) and Computer Vision (CV) more generally indicate that methods alike should be taken in consideration and further analysed and developed.

For the first part, we will start off with an overview of the current problem space and the argument necessity of studying such techniques. Following this, Chapter 2 begins by providing extended details regarding the current state of research for GIS starting from characteristics of Remote Sensing data to how the acquisition of such data is performed and to additional preprocessings that could be required. Within Chapter 2 we also present informations about the inner workings of ML with respect to current heuristics that are used in the literature for solving various CV tasks.

Chapter 3 showcases the approach taken for developing an appropriate multi-modal spatio-temporal Remote Sensing dataset publicly available data. Some results on experimenting with ML techniques for training Convolutional Neural Networks (CNN) on the task of semantic segmentation of vegetation related classes are also presented for validating the usability and relevance of the aforementioned dataset.

Chapter 4 illustrates the results of training such models on the proposed dataset on how they perform on solving the task of semantic segmentation of vegetation.

Abstract

Recent, industria geospațială s-a dezvoltat într-un ritm constant. Această creștere implică și adăugarea unor constelații de sateliți care produc zilnic o cantitate impresionantă de imagini satelitare dar și a altor tipuri de date specifice teledetecției. Uneori aceste informații, chiar dacă în unele cazuri ne referim la date publice, nu sunt folosite din cauza volumului acestora. Procesarea unor cantități impresionante de date folosind resurse umane sau metode clasice de automatizare nu este întotdeauna o soluție viabilă din punct de vedere al timpului și al resurselor necesare.

În acest document, propunem o abordare pentru crearea unui set de date variat, spațio-temporal compus din date achiziționate prin tehnici de teledetecție, dar și testarea fezabilității acestuia folosind dezvoltări recente din domeniul învățării automate (ML). Mai precis, utilizarea rețelelor neuronale convoluționale (CNN), care sunt capabile de separarea diferitelor clase de vegetație din setul de date propus. Popularitatea și succesul metodelor similare în contextul sistemelor geografice informaționale (GIS) și în general în domeniul Computer Vision (CV) indică faptul că metode similare ar trebui luate în considerare și analizate.

În prima parte, vom începe prin a prezenta o viziune de ansamblu a spațiului curent al problematicii și vom argumenta necesitatea studierii tehnicilor de învățare automată. Ulterior, Capitolul 2 prezintă detalii extinse legate de starea actuală a literaturii de specialitate atât pentru GIS, începând cu unele caracteristici ale datelor preluate prin tehnici de teledetecție până la cum are loc procesul de achiziție al datelor la preprocesări adiționale ce ar putea fi necesare. Capitolul 2 include de asemenea informații despre cum funcționează tehnicile de învățare automată vizavi de euristici folosite în prezent pentru rezolvarea a diferite sarcini în domeniul Computer Vision.

Capitolul 3 prezintă abordările luate în dezvoltarea unui set de date multi-temporal și spațio-temporal cu informații preluate din teledetecție. Rezultatele experimentelor folosind tehnici de învățare automată prin antrenarea unor Rețele Neuronale Convoluționale (CNN) pentru a segmenta semantic imagini satelitare în concordanță cu clase de vegetație pentru a valida setul de date antemenționat.

Capitolul 4 ilustrează performanța modelelor folosind setul de date menționat, arătând eficiența lor în rezolvarea problemei de segmentare semantică a vegetației.

Contents

1	Introduction	8
1.1	Remote sensing	9
1.2	The Copernicus programme	10
1.3	Artificial Intelligence Techniques	10
1.4	Motivation	11
2	State of the Art	14
2.1	Data acquisition techniques	14
2.2	Remote Sensing centric datasets	15
2.2.1	SpaceNet Roads and SpaceNet Buildings	15
2.2.2	BigEarthNet	15
2.2.3	Corine Land Cover (CLC)	16
2.2.4	MODIS Land Cover	17
2.2.5	LUCAS	17
2.2.6	EuroSAT	18
2.3	Machine Learning in the context of Computer Vision	19
2.3.1	Image Classification, Localization, Object Detection, Instance Segmentation and Semantic Segmentation	20
2.4	Convolutional Neural Networks	22
2.4.1	Backpropagation: How are Neural Networks trained?	22
2.4.2	Common layers of CNN	23
2.4.3	Optimizers	27
2.4.4	Fully Convolutional Neural Networks	28
2.4.5	SegNet	29
2.4.6	U-Net	31
2.4.7	ResNet	33
2.5	Measuring the performance of models	34
2.5.1	Accuracy: is it enough?	34
2.5.2	Precision & Recall	34
2.5.3	F-score / Sørensen-Dice coefficient	35
2.5.4	IoU/Jaccard index & MIoU	35
2.6	Multi-modal learning	36
2.7	Introducing Hugin: Machine Learning using remote sensing data	37
3	Semantic segmentation of vegetation in Remote Sensing imagery: an approach based on Machine Learning	38
3.1	ESA DHuS as a data source	39

3.1.1	Extracting data from DHuS	39
3.1.2	Current limitations of DHuS and alternatives	39
3.2	Sentinel-2 and Sentinel-3 archives	40
3.3	Data preprocessing	40
3.3.1	Reprojecting Sentinel-3 archives using ESA GPT	40
3.3.2	Corine Land Cover rasterization	41
3.3.3	Cloud masks - Sen2Cor	41
3.3.4	Tiling and mosaicking	41
3.4	Constructing a multi-modal dataset	41
3.4.1	Zarr as a data storage format	42
3.4.2	Splitting the dataset: Stratified K-folds	43
3.5	Training Convolutional Neural Networks with Hugin	44
4	Experiments	45
5	Conclusions	47
	Bibliography	52
A	Remote Sensing	53
B	Sentinel-3 GPT preprocessing	58
C	Hugin configuration examples	59
D	Additional experiments results	61

Chapter 1

Introduction

As of relatively recently, the world has started to become increasingly reliant on technology that implements Artificial Intelligence techniques. From automating labor-intensive tasks, to offering aid in medical diagnoses, to autonomous vehicles, anticipating stock market prices, automatically scaling cloud infrastructures based on predicted demand, natural language processing, data fusion, enhancing image resolution (also named super resolution), image segmentation. The aforementioned are some particular examples of tasks the realm of Artificial Intelligence can offer aid in. There is no doubt about the benefits that a certain subdomain of this field of study, namely Machine Learning (ML) is adding to our day-to-day life. We can argue that the increase in popularity for these types of methods is due to the timeframe we live in. Never has the production rate of data been so considerable than now. We are referring of course, to the Big Data phenomenon. The context in which data is being generated varies. If we are talking about Web 2.0, then we are talking about user generated data, mostly popular nowadays being social media platforms (contents usually include: pictures, videos, audio or text). Some other examples of data sources can be machine generated, such as measurements from sensors, performance and usage logs extracted by using monitoring techniques on cloud and IoT infrastructures. All of those modern requirements to process large quantities of information have greatly influenced the evolution of Artificial Intelligence. Previous methods of achieving similar tasks, such as expert systems required more focus on defining rules manually (based on the available data) for the system to follow in order to perform reasoning. Nowadays it is nearly impossible to create such rules due to the volume and variety of the data at hand. The goal of Machine Learning algorithms is to automatically generate rules based on the data.

For the purpose of this thesis, we will however focus on the niche of Computer Vision (CV). More precisely, on applying Machine Learning to satellite imagery that was collected through remote sensing techniques (detailed in Section 1.1). We will use a class of ML techniques called supervised learning, which assume that we feed the algorithms with concrete examples (labeled data) of what the input looks like, while also describing the desired output. Therefore, a ML model needs to learn a correlation between the two. Computer Vision itself, is a branch of Artificial Intelligence, and is the discipline dealing with analyzing and interpreting digital images and videos (examples of tasks belonging to CV, are detailed in Section 2.3.1).

1.1 Remote sensing

Generally, by Remote Sensing we understand the process of acquiring information about the physical characteristics of land surfaces, by utilising methods that do not require direct human contact. As of recently, this industry for both the public and private sectors has seen a steady growth, being an active participant in the big data phenomenon as a data source. Observing the Earth is becoming more important now than ever. With the availability of high quality Remote Sensing data, also comes a research interest that has been growing in the last three decades according to a bibliometric analysis performed on Clarivate's Web of Science database [11].

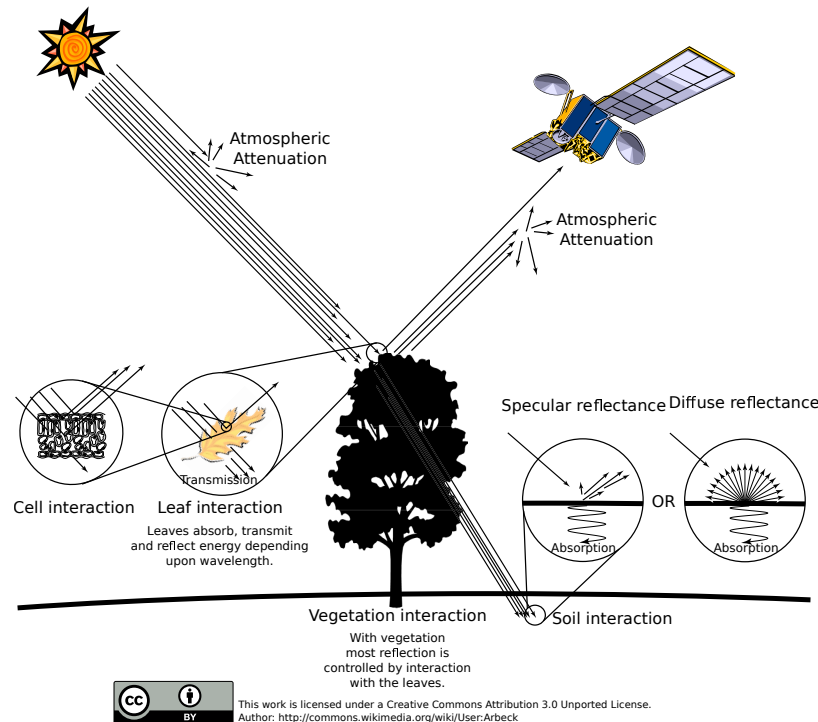


Figure 1.1: A typical passive Remote Sensing environment

There are two categories of remote sensing: either active, or passive, depending on how the acquisition process is done. If the sensors that are used for measurements do not emit radiation, and natural sources such as the Sun energy reflections (visible and infrared wavelengths) are collected by the sensors, then the process is passive. On the other hand, if sensors are used also for emitting radiation towards the area of interest, whose backscatter¹ will later be collected, then the process is active. Figure 1.1 illustrates the passive process, and Figure A.1 shows the difference between active and passive Remote Sensing. Data acquisition can be performed using multiple instruments: SAR, LiDAR, MSI, and OLCI (Section 2.1) are some of them.

Remote sensing has a wide variety of usecases. Examples include: monitoring land cover or land usage, detecting changes in land coverage, tracking phenomenas with impact on land surface like floodings, movement of glaciers, earthquakes, or forest fires, tracking cloud formations for weather forecasting. The domain also encompasses oceanography, which includes tasks like: scanning the ocean floor, and keeping track of ocean color, turbidity, temperature and other specific properties.

¹Reflection of signal back to the source.

1.2 The Copernicus programme

Copernicus^{2,3} is a collaboration between the European Space Agency (ESA) and the European Commission (EC). It’s aim is to create a powerful Earth Observation (EO) programme, starting from launching and controlling of satellites to collecting, processing and distributing the collected data to delivering software products.

By launching the Sentinel family of satellites (see Sections 3.2,3.2 for two specific examples), the programme is able to provide easy to access accurate, and high quality remote sensing data. This data ranges from radar and multi-spectral imaging for land monitoring, ocean and land cover data, to atmospheric composition information. Part of the data from the Copernicus programme is being made available through the Data Hub Software⁴ (DHuS). The Data Hub Software was used in the scope of this work as well, as it was a primary source for the dataset. Sentinel-2 and Sentinel-3 archives were downloaded in specific, as detailed in Section 3.1.

1.3 Artificial Intelligence Techniques

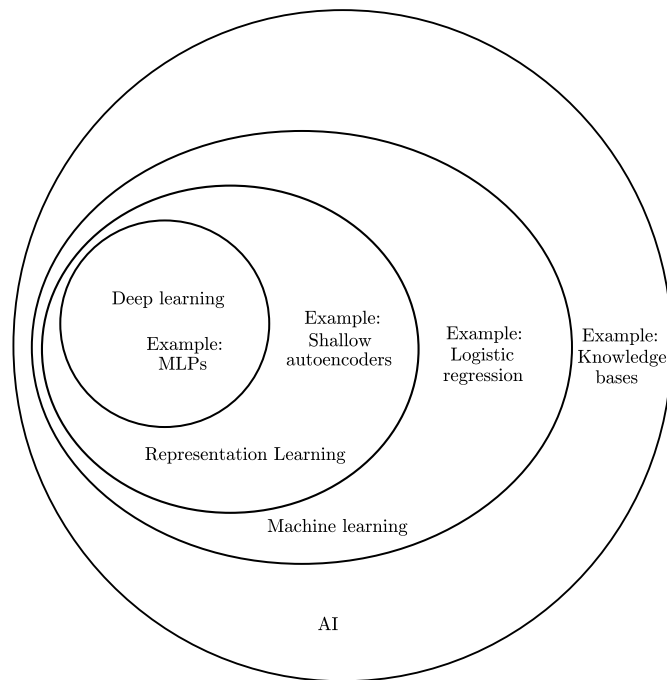


Figure 1.2: Artificial Intelligence and it’s subfields [14]

The Venn diagram illustrated in Figure 1.2 provides us with the context of the current work, with each subset of the Artificial Intelligence superset representing a different branch/subdomain. The methodologies that are to be used in the current work reside in the inner-most set, that of Deep Learning. MLP or Multiple Layer Perceptrons are a prominent example of this branch, and they represent the atomic

²https://www.esa.int/Applications/Observing_the_Earth/Copernicus/Overview3

³Previously named “Global Monitoring for Environment and Security” (GMES)

⁴<https://github.com/SentinelDataHub/dhus-distribution>

building block that is used to structure each ANN (Artificial Neural Network). One such class of ANN that is used extensively in the field of Computer Vision are Convolutional Neural Networks (CNN), which are to be described into detail in Section 2.4. The outer-most layer (knowledge bases) and some shortcomings when they are used to process larger volumes of data were presented. But what about the other three layers? Should the terms “Machine Learning” and “Deep Learning” be used interchangeably? Answers to the latter question might vary. There are two main differences between the two. They have to do with the structure of the data, but also with how the learning process is achieved. With Machine Learning, we can for instance provide labeled input images. The model is trained in order to progressively get better at the task of classifying images based on labels (correlation of input-output). It can only take into account the global context of the image we are providing in order to determine the features that dictate what label it should assign to it. Deep learning assumes there exists an hierarchy of layers, each of it being able to determine local features within the image that will build up the reasoning behind choosing the class an image belongs to. Furthermore, they can be extended with the help of Softmax (Section 2.4.2.4) into providing a probability vector regarding the belonging of a particular input to a class, or to what the problem at hand might be. This is in contrast to another type of CNN, namely Fully Convolutional Networks (FCN) where the last layer is replaced by a convolution one instead of Softmax or other classifiers. There is an importance of how data is represented and given to a Machine Learning model. Sometimes there is the possibility to hand-pick or craft⁵ the features which are to be fed to the model. But in the case where this is not possible and representation becomes more complex such as when dealing with comprehending images or videos or processing natural language, Representation Learning is a viable choice. Representation Learning provides ways of automatically learning feature representations. Common ways of learning such representations are autoencoders (where representation is learned separately from labeled data⁶). Approaches based on encoder-decoder topologies (some examples are discussed within Chapter 2) use said encoders for mapping inputs to feature representations, while also using them in the decoder for taking informed decisions.

1.4 Motivation

This section provides an answer to an important question: “*What do we have to gain from using Machine Learning with this kind of data?*”. Presuming the proposed task is being executed successfully (i.e. the models being able yield a satisfactory performance⁷ in respect to semantic segmentation) there are numerous benefits within the realm of Remote Sensing and Geographic Information Systems (GIS) in particular. While also having an impact on the human decision-making process regarding organizational measures in general.

Focusing on the task of semantic segmentation (Section 2.3.1) in Remote Sensing imagery, the end result, the prediction masks (or segmented images) provide an overview of land usage/land cover. In this work, the prediction masks are displaying

⁵This is also known as “feature engineering”.

⁶Therefore, autoencoders are categorised as unsupervised learning.

⁷In comparison to similar results of methods that are in the same class of problems

the composition and diversification of vegetation in the images given to the model.

Before going further, there are some explanations to be done about the two terms mentioned in previous paragraphs. Although land use and land cover are sometimes used interchangeably, they refer to distinct issues. The first term's meaning is that of how parts of the Earth's surface are being used by the population, and it is related to socioeconomic aspects as well. The latter's is strictly referring to the physical composition of the surface of Earth. In both cases, the end product, usually called an inventory, is comprised of a set of labels, which are associated to real-world surfaces within the area of interest in which the study was conducted on.

The current proposal falls into the category of land coverage. Typically land cover information is collected by one of two means: either through land surveys or through Remote Sensing techniques. There are two examples of such inventories, which are to be discussed in Chapter 2. Namely, we are talking about the LUCAS[4] dataset that was created through land surveys conducted by an initiative of Eurostat. On the other hand Corine Land Cover (CLC)[7] is a land cover inventory created with the availability of Remote Sensing imagery (by using multiple satellites such as Landsat, SPOT and since 2018 Sentinel-2 and Landsat-8). The data was later inspected, and the inventory was generated by using semi-automated GIS methods.

Typically, land cover and Remote Sensing in general are considered to be sub-domains of geography. Previous approaches to process remote sensing data were performed either manually by cartographers (e.g. in the case of CLC [7]), or with the help of morphological transformations [32, 26]. Morphological transformations are a set of mathematic operations, which are usually applied to images in order to perform various processings. While these techniques yield satisfiable performance, they are limited in terms of the variety of tasks they can perform. It is also common for morphological transforms to be used in conjunction with artificial intelligence [6] in order to preprocess or postprocess data, thus enhancing the performance of models.

Once obtained, information about land coverage can be of use in multiple different applications. Most of which are concerns that qualified institutions are expected to work with as part of their expertise. This list includes:

- Environmental planning
- Monitoring the effects of climate change
- Disaster management and risk assessment
- Environmental predictions
- Management and preservation of wildlife

All of the aforementioned applications are dependent on information concerning the physical coverage of a given area of interest. Appendix A provides additional details about the land cover on the territory of Romania, providing further motivation for studying changes land cover for vegetation. The current work proposes a method for extracting land cover inventories automatically, with interest in vegetation coverage by using remote sensing data with the help of modern artificial intelligence.

A short description of the problem

The current work contains some proposals for developing Machine Learning models that have the capability to differentiate between different types of vegetation using a new multi-modal and spatio-temporal dataset comprised of Remote Sensing data.

There exist limitations regarding the current state of the art in both Artificial Intelligence, and with the data that is to be processed. For example: even if desired, it is not possible to obtain a finer granularity over the number of classes that we predict, if our dataset does not contain concrete examples for more classes (i.e. the classes that we train our model with, are also the ones that it outputs in predictions).

The simplest example of what the goal of the current work is illustrated within Figure 1.3. Based on a given input, in this context a satellite image, through using Machine Learning techniques, we are to be able to generate a prediction mask indicating the types of vegetation that exist in the image and where they reside.

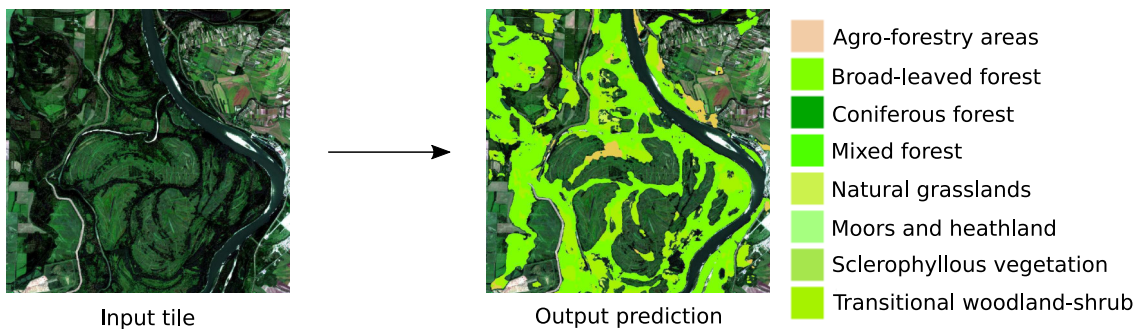


Figure 1.3: Example of semantic segmentation of forestry in Sentinel-2 RGB data
Images extracted from LeafS project developed for FOSS4G 2019 EO Data Challenge

Objectives of the current work

- Creating a multi-modal (Section 2.6) dataset covering the area of Romania.
- Training of various Machine Learning models based on convolutional neural network topologies (Sections 2.4.5, 2.4.6, 2.4.7) using Hugin (Section 2.7) on the task of semantic segmentation for the vegetation classes from CLC using the aforementioned multi-modal dataset.
- Analyzing the results and comparing the performance yielded by these models.

Chapter 2

State of the Art

The current chapter provides an overview of current literature in both Artificial Intelligence and Remote Sensing, focusing on techniques that are used in Chapter 3.

2.1 Data acquisition techniques

As briefly mentioned in Section 1.1, there are various instruments on board of satellites. For the purpose of the current work, we want to focus on two of them: MSI (Multi-Spectral Imagery) provided with Sentinel-2 and OLCI (Ocean and Land Colour Instrument) from Sentinel-3. These instruments provide information about land coverage that can be useful when detecting vegetation in Remote Sensing data.

The Sentinel-2 MSI¹ data contains 13 spectral bands at different spatial resolutions (4 bands at 10m resolution, 6 at 20m and 3 bands at 60m). Various types of vegetation can be identified based on their signature, that is the spectral response collected as backscatter by the satellite’s instruments. Data is distributed via the DHuS in different processing levels. In the case of Sentinel-2 MSI there are three processing levels, but only two are publicly available. Level-0, Level-1 and Level-2 each including different stages of processing. Level-2 data is the most “complete” in terms of processing, consisting of BOA (Bottom of Atmosphere) reflectance images that are georeferenced in the UTM grid projection. The granularity of a Sentinel-2 MSI Level2-A scene (or tile) is $100 \times 100 \text{ km}^2$. Sen2cor [24, 3] is further used in order to process Sentinel-2 archives and also detect clouds, cloud shadows and snow. This method is helpful to take into consideration when using Machine Learning, as portions of images that are occluded by clouds can interfere with training models.

The Sentinel-3 mission also provides data from the OLCI² instrument. At a 300m spatial resolution, a product is composed of data from 21 spectral bands, quality control flags, tie points and information regarding georeferencing. The 21 bands encompasses different functions ranging from chlorophyll absorption, sediment loading, chlorophyll fluorescence levels, water vapour absorption levels to aerosol corrections and atmospheric corrections. This information makes Sentinel-3 OLCI a good instrument for identifying signatures of vegetation in land coverage.

¹sentinels.copernicus.eu/web/sentinel/user-guides/sentinel-2-msi/overview

²sentinels.copernicus.eu/web/sentinel/user-guides/sentinel-3-olci/overview

2.2 Remote Sensing centric datasets

In the context of Remote Sensing, several datasets are present in the literature and are publicly available. Most of them have been created with the purpose of helping building automated methods that give aid in identifying the land coverage or usage.

Two most common ways of storing GIS data are by using either vector or raster formats. With vector formats, information is stored based on drawn shapes (such as points, lines, polygons) using geographical coordinates as a spatial reference. Vector formats typically store discrete values. Raster is a matrix like structure that contains features usually stored as continuous values, with a fixed spatial resolution. Vectorial dataset examples include CLC and LUCAS, while BigEarthNet, MODIS, EuroSAT and SpaceNet contain raster data. Rasterization is the process of converting vector format data into raster data (as exemplified within Section 3.3.2).

2.2.1 SpaceNet Roads and SpaceNet Buildings

In the context of a competition, CosmiQ Works in collaboration with Amazon have published the SpaceNet [33] dataset. The objective in this competition is to create ML models that yield a good performance for binary semantic segmentation of road networks or buildings, or for monitoring urban development over time. The dataset contains more than 10.500km of road structures and 811,982 polygons marked as buildings. SpaceNet7 includes 24 satellite imagery mosaics representing a timeframe of 24 months covering over 40.000km² representing urban development.

The dataset is composed of RGB and multi-spectral WorldView2 and WorldView3 imagery at a spatial resolution of 30, respectively 50 centimeter. Besides the input images, ground truth labels are provided as GeoJSON and they have been extracted from OpenStreetMaps and manually checked to correspond to real road networks or building structures. The competition is developed to increase in complexity with each iteration by adding more requirements, such as estimating the time it takes to traverse a predicted road network or by adding off-nadir³ and very off-nadir images.

2.2.2 BigEarthNet

BigEarthNet [30], a recently published remote sensing image benchmark dataset, is composed of 590,326 tiles which were extracted from 125 Sentinel-2 MSI archives. The tiles have different spatial resolutions (126x126 for the 10m bands, 60x60 for 20m bands, and 20x20 for the 60m bands). This dataset is specifically designed for training and comparing the accuracy of deep learning models (benchmarking). The sensing period of the data ranges from between June 2017 and May 2018, and the Area of Interest (AOI) covers 10 European regions (namely Austria, Belgium, Finland, Ireland, Kosovo, Lithuania, Luxembourg, Portugal, Serbia and Switzerland).

Each image is annotated with one or more labels from the Corine Land Cover inventory (Section 2.2.3). The absence of segmentation masks and small tile sizes make BigEarthNet better suited for training ML models in order to solve the task of image recognition (or classification) rather than for solving semantic segmentation.

³By nadirness, we understand the various angles of the satellite in relation to the target at the moment of acquiring the images. Nadir (< 25°), off-Nadir (> 25°, < 40°), vert off-Nadir (> 40°).

2.2.3 Corine Land Cover (CLC)

Corine Land Cover⁴ is a popular land cover/land use inventory created within the context of ESA's Copernicus Land Monitoring Service. It mainly consists of a hand-mapped (based on raster interpretation) package of polygons belonging to 44 different land cover classes for countries that are either part of the European Union, or who volunteer to provide data. There are some countries have used semi-automated methods to create their inventory (Germany, Ireland, Spain, Portugal).

The inventory exists since 1990, and the latest remapping has been performed in 2018. A variety of different satellite data has been used as guides for it's creation: 1990 - Landsat-5 (50m spacial resolution), 2000 - Landsat-7(25m), 2006 - SPOT-4/5 (25m), 2012 - IRS P6 LISS III and RapidEye (25m), and the latest, 2018 - Sentinel-2 (10m). Changes in land coverage are also distributed separately in CLC. The minimum cartographic unit (MCU) in CLC is 25ha, and the accuracy of the mapping is better than 100m. Data within the inventory is stored as a hierarchy on three levels based on grouping of classes, as mentioned in the nomenclature [12].

The extents of this inventory (39 countries partaking in the effort by 2018) as well as the fact that the inventory is performed and published periodically and changes in land cover are marked separately together with the variety of existent classes make Corine Land Cover a viable choice for using it as ground truth data when investigating land coverage, usage or change detection on the European continent.

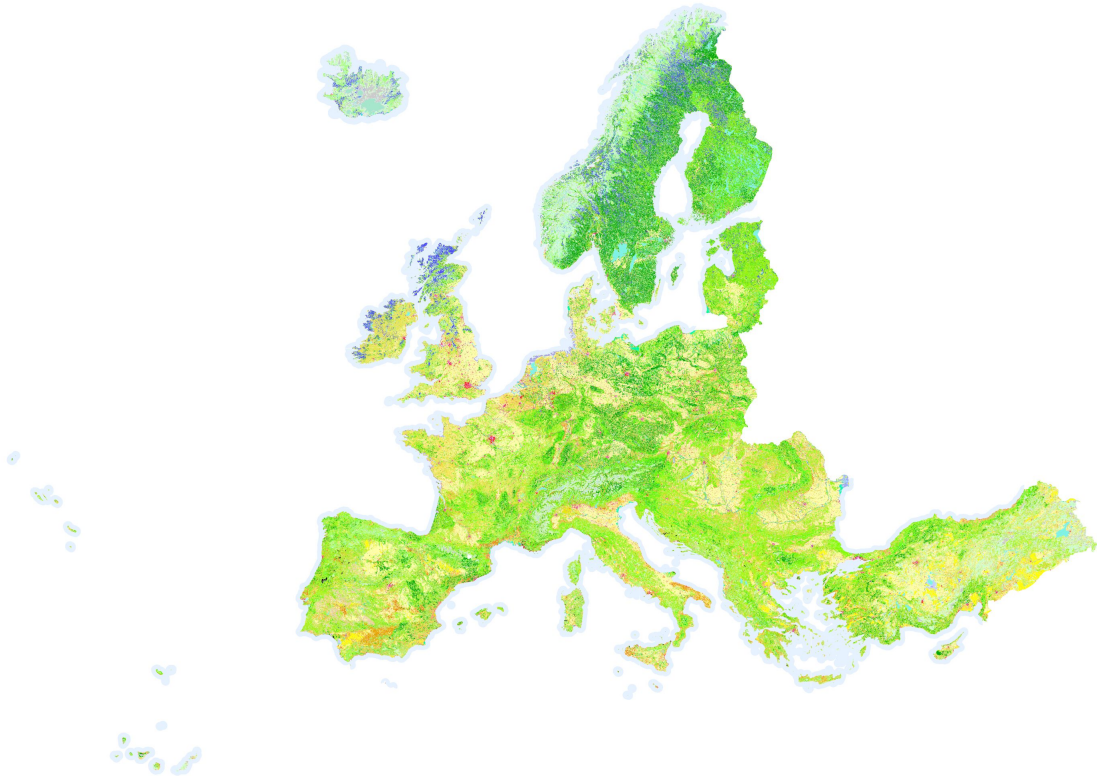


Figure 2.1: Extents of the Corine Land Cover inventory

⁴<https://land.copernicus.eu/pan-european/corine-land-cover>

2.2.4 MODIS Land Cover

Similarly to ESA’s effort in the field of land monitoring and land cover, NASA also releases the Moderate Resolution Imaging Spectroradiometer (MODIS) Land Cover product [29] (or MCD12Q1). Currently at it’s 6th version, this inventory has been released annually since 2001. It is composed of 13 datasets, which spread hierarchically on 5 different classification schemes (they are shown in Figure 2.2). The datasets also include layers for quality assurance and a binary land-water mask.

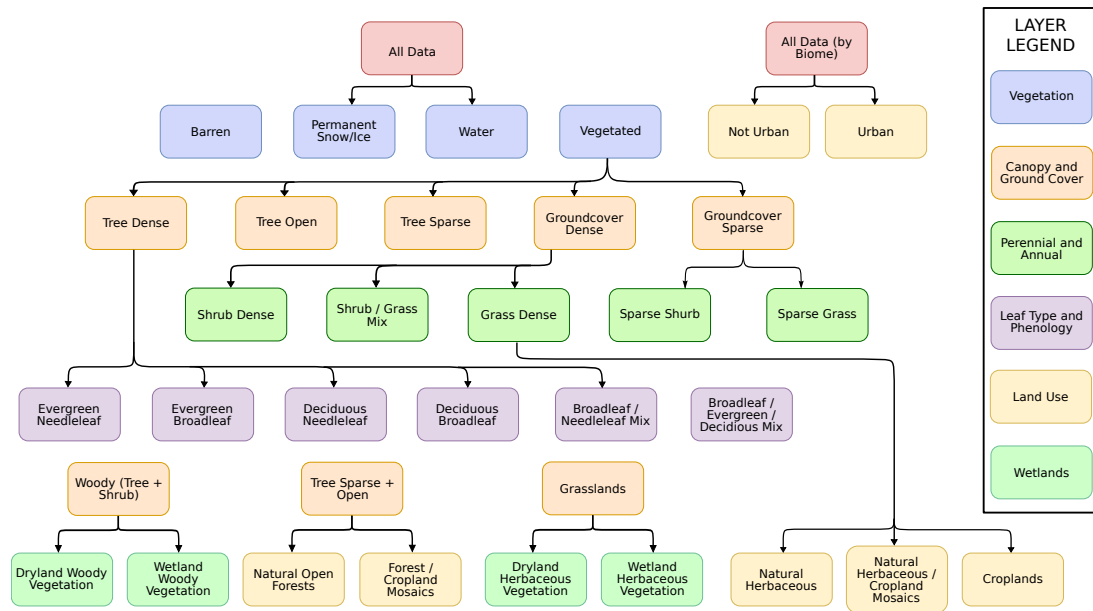


Figure 2.2: MODIS Land Cover classes hierarchy [29]

The MODIS MCD12Q1 land cover inventory is created with the help of classification models [13] using reflectance data acquired worldwide from the MODIS instrument. The inventory that is derived from these models has a spatial resolution of 500m.

2.2.5 LUCAS

LUCAS [4] or Land Use and Coverage Area frame Survey performed by Eurostat⁵ for mapping changes in land coverage and land usage over time for the entire territory of the European Union. This survey has been taking place regularly at a 3 year interval since 2006 (although the LUCAS initiative has been in existence as of 2001).

The land cover and use data in the LUCAS inventory is collected manually. This means that surveyors have to physically assess the landscape within the AOI (also called “*in situ*”) in order to determine the coverage and usage and even take soil samples to be further examined⁶. Besides having to determine land cover/use, the surveyors also take photographs in the 4 cardinal directions. Data acquired by the surveyors is photo-interpreted and land cover/use in any given point is classified from a catalog of 8 categories, 29 classes and a total of 76 subclasses. Data was collected at points at a distance of 2 kilometers to each other and the survey contains a total of around 1.1 million such points in which observations were made [4].

⁵<https://ec.europa.eu/eurostat/home>

⁶<https://ec.europa.eu/eurostat/web/lucas/overview>

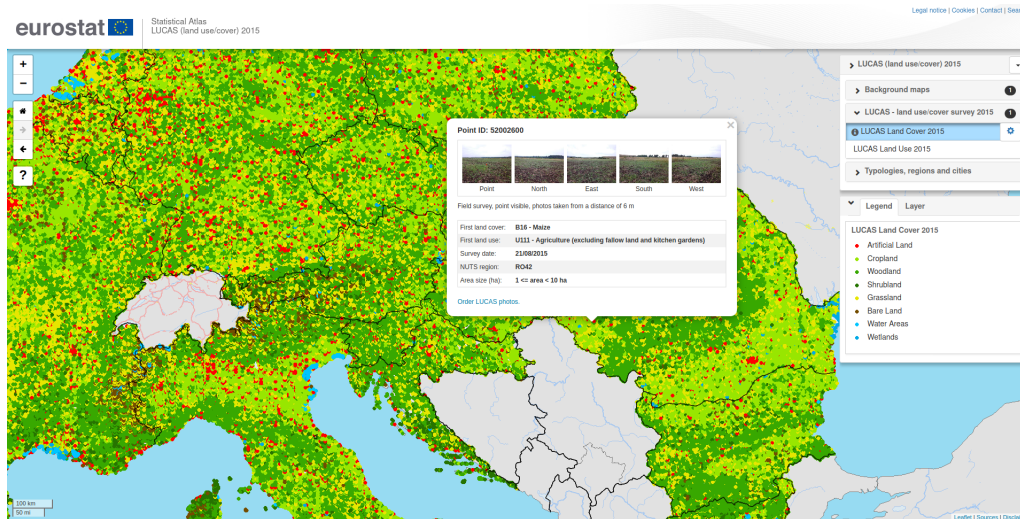


Figure 2.3: Screenshot of LUCAS Statistical Atlas

Access to the data acquired from the LUCAS survey is achieved through the web portal⁷ (Figure 2.3). The data that’s being made available consists of aggregated statistical tables and individual points data (images, classes of land cover and use).

Overall, with the fact that the data is collected manually presents an advantage in the context of building ML models, since the ground truth data is highly accurate.

2.2.6 EuroSAT

EuroSAT [16] is a benchmarking dataset designed for identifying land usage and land coverage. Composed out of 27.000 Sentinel-2 MSI imagery that have been labeled using 10 land cover classes. Satellite imagery for 34 countries located in Europe (that are associated with the European Urban Atlas⁸) that contain a small cloud coverage have been hand picked. The size of an image patch found in EuroSAT is 64x64 pixels and the labels have been extracted from the European Urban Atlas.

For statistical relevance, EuroSAT data was picked uniformly throughout the year of 2019 and each land cover class has about 2000-3000 samples spread across cities from the 34 countries. Benchmarking and proof of the relevance was performed using ML techniques [16], namely by using CNN for listing classification accuracy. More precisely, EuroSAT [16] has been validated by using the ResNet-50 [15] and GoogLeNet [31] topologies for classifying land coverage on different splits of data.

Due to the small size of patches (64x64 pixels) and the absence of segmentation masks, EuroSAT [16] is similar to BigEarthNet [30]. This means it also has a good potential for using it as a benchmarking dataset to be used for solving problems such as classification of land cover classes, but it is not ideal for semantic segmentation.

⁷<https://ec.europa.eu/eurostat/statistical-atlas>

⁸<https://land.copernicus.eu/local/urban-atlas>

2.3 Machine Learning in the context of Computer Vision

The primary goal in Computer Vision is to be able to automatically interpret and understand image and video content mimicking as closely as possible the human process of interpreting vision. The usage of Artificial Intelligence techniques such as Machine Learning can provide aid to in understanding this type of content.

Even if Machine Learning, especially applied in the field of computer vision is a hot research topic, it is a fairly mature field. Nowadays, Approaches regarding Deep Learning techniques, especially Convolutional Neural Networks such as the ones shown in Sections 2.4.5, 2.4.6, are popular amongst research within the field of CV.

Most tasks in the field of Computer Vision are solved with the help of supervised learning methods such as Convolutional Neural Networks proven to yield satisfactory results. Using supervised Machine Learning techniques to solve Computer Vision tasks such as the ones described in Section 2.3.1 also comes with difficulties. These difficulties are discussed within Section 2.3.1.1. Since research in the field of CV is popular, methods for mitigating those difficulties are also known to exist.

With the appearance of datasets specialized to provide aid in CV, some examples including: ImageNet [10], CIFAR [20] or MS-COCO [22], solving tasks (Section 2.3.1) using supervised ML approaches, especially by using CNN has been widespread. Although there are numerous specialized datasets that are ready to provide aid in training automated techniques to perform on Computer Vision tasks, there is numerous content being generated on a daily basis from Web2.0, satellites, and generally simple cameras, most of this data is not labeled in a way to permit supervised Machine Learning. Development of datasets is an important part of contributing to both the fields of Computer Vision and Machine Learning.

Some datasets are distributed in centralized places, such as on the Kaggle⁹ platform which is destined to create competitions for developing automated methods for solving tasks. Kaggle hosts numerous CV competitions which have labeled datasets for performing supervised learning.

Applications of Machine Learning in the context of Computer Vision varies to a multitude of domains, ranging from building autonomous vehicles (which include detection of traffic signs, road condition monitorization, traffic monitoring, pedestrian detection), providing aid in medical diagnosis by interpreting images taken from different medical aperture, facial detection and recognition, monitoring of crops, to changes in vegetation and urban development.

⁹<https://www.kaggle.com/>

2.3.1 Image Classification, Localization, Object Detection, Instance Segmentation and Semantic Segmentation

There are multiple different problematics to be solved within the field of Computer Vision, and also, some open problems as well. The most popular tasks are illustrated within Figure 2.4. Due to the fact that the goal of the current work (i.e. Semantic Segmentation) is built upon knowledge from the other tasks, we will provide an explanation for what each of those suppose and the key differences between them. Although these task might seem trivial to solve at first, the open problems such as those listed within Section 2.3.1.1, or the existence of adversarial patches [8] make solving Computer Vision tasks significantly more difficult.

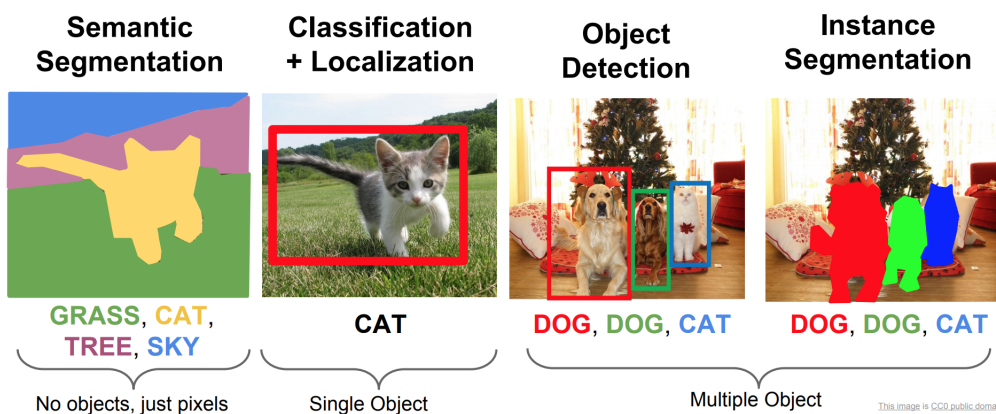


Figure 2.4: Comparison of the four common tasks in Computer Vision [19]

Classification is when an image is assigned a single label¹⁰ representing the most prominent object contained in an input image. As illustrated in Figure 2.4. A couple examples of well-known datasets which are specifically constructed with tasks such as classification in mind are: CIFAR [20], ImageNet [10] or MS-COCO [22].

Classification with localization in addition to simple classification, localization also encompasses the drawing of a bounding box over a section of the original input image. Therefore strictly encasing the one object that was classified by the model.

Object detection is about classifying multiple objects from a single input image. This detection is done in the style of localization. The output is then comprised of multiple bounding boxes and labels corresponding to the detected objects.

Instance segmentation is similar to object detection, but with some additions. Instead of having bounding boxes, the output now is a pixel mask over the image. Most important, it adds the ability to distinguish between objects of the same class.

Semantic segmentation refers to partitioning a given input image into regions of pixels which cover each of the different classes that compose the image. The output in semantic segmentation is, again, a mask of pixels with the size being equal to the one of input image. This task is what we want to adress in respect to Remote Sensing data in order to accurately classify different classes of vegetation (available within the Corine Land Cover inventory - see Section 2.2.3). Furthermore, the methods used to approach the problem are described within Chapter 3.

¹⁰From a given, fixed set of labels that we train a model with.

2.3.1.1 Challenges in Computer Vision

There are numerous problems that interfere with solving the problems that we're presented in Section 2.3.1. All of them have to do with the nature of the data that we have available. These problems are also encountered in Remote Sensing imagery.

Some open problems within Computer Vision include:

- **Viewpoint variation** is when an image of an object is acquired at different orientations in relation to the device that acquired the image.
- **Scale variation** happens when instances appear at varied sizes not due to the extents of the image, but to their real-world size.
- **Deformation** where real-world objects appear distorted in the images.
- **Occlusion** happens when the object of interest is either partially or almost totally covered by another object.
- **Illumination variation** are changes in the lightning conditions of images. They can also create issues when there are significant changes of it throughout examples within a dataset.
- **Background clutter** sometimes, it could be difficult even for the human eye to distinguish objects within a cluttered image.
- **Intra-class variations** refer to the dissimilarities between instances of the same class. Instances that are part of the same class might look very different.
- **Adversarial patches** [8] present an interesting approach: generating patches from an image (usually, an image containing a random object) with some specific means of distortion and applying them to an image that is going to be fed to a Machine Learning model to predict. The goal here is to purposefully trick the model into miss-classifying the object found in the image.

With the exception of adversarial patches, these are shown within Figure 2.5.

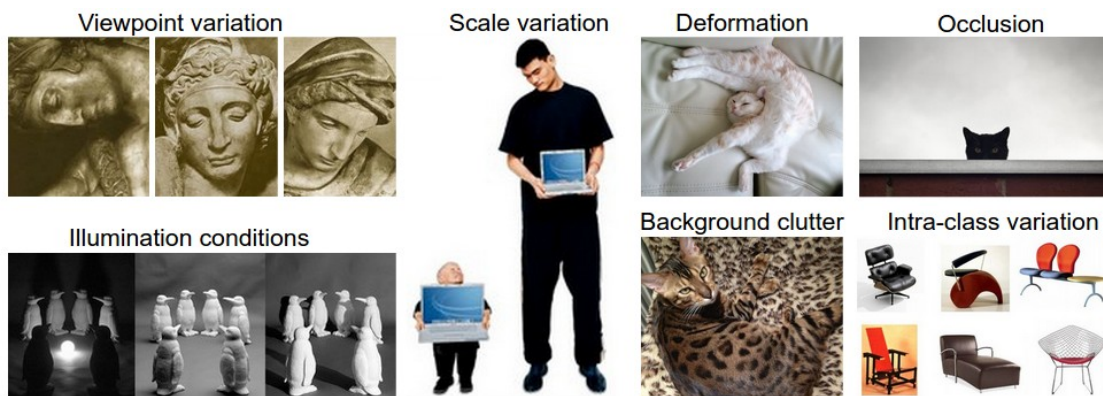


Figure 2.5: Challenges in Computer Vision [19]

The challenge that is most encountered when working with Earth Observation data is occlusion. Mainly, this problem appears especially when working with RGB

imagery and cloud formations are the objects that are occluding data. There exist several approaches which help mitigate the problem such as creating cloud masks [3] in order to take occluded data into account when training models. These techniques have been extracted from the literature and discussed are within Section 3.3.3.

2.4 Convolutional Neural Networks

Convolutional Neural Networks (CNN) are a class of deep learning networks, that are widely used on matrix-like data. They have been introduced to the literature ever since 1989 with the purpose of classifying hand-written zip-codes [21]. Convolutional Neural Networks are organized in a multiple layer perceptron (Figure 2.6) fashion (i.e. there exists one input layer for the data, followed by multiple hidden layers containing different operations, which are described into detail in Section 2.4.2, and finally, at the end of the topology there exists an output layer).

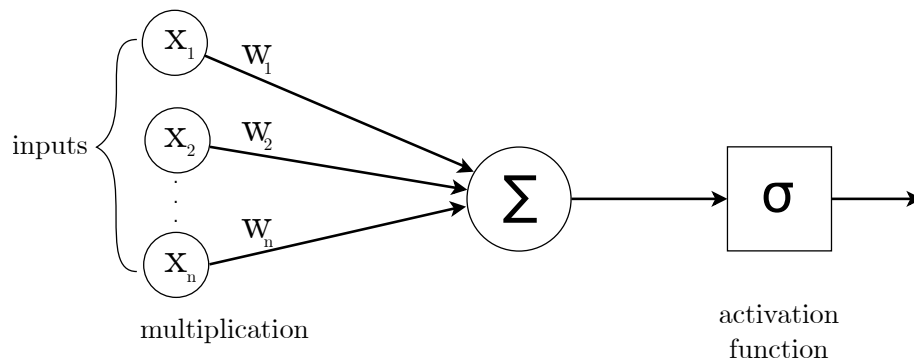


Figure 2.6: Example showing a perceptron, the principal building block of CNN's.

These perceptrons are the virtual equivalents of human neurons, and in a typical neural network, they are aggregated to pass their output as input for the next layer of perceptrons. The basic functioning principle of multi-layer perceptrons is that, for the first layer of the network (i.e. the input layer) the input vector $[x_1, x_2, \dots, x_n]$ corresponds to the values of the input data (typically the values of an image from the dataset). These values are multiplied by weights $[w_1, w_2, \dots, w_n]$ which are modified by the training algorithm, called backpropagation (Section 2.4.1). The weighted sum is passed to an activation function (Section 2.4.2.5) that decides if the perceptron is or not to be activated (i.e it contributes to the reasoning process).

2.4.1 Backpropagation: How are Neural Networks trained?

Backpropagation is the algorithm used for training a certain class of ANN, namely feedforward neural networks (meaning that the connection between perceptrons in the network are unidirectional and acyclic). Since an ANN is comprised of multiple layers of perceptrons, we have multiple weights between these layers. We also receive an input vector x , and we want to create an association between the input x and the output y . The goal of backpropagation is to understand how to adjust the biases and the weights between layers in order to minimize the error of a model (calculated by an error function). The error is therefore calculated as a difference between what a model predicts (y_i) and what the example in the training dataset actually is (\hat{y}_i).

Underfitting and Overfitting

In the context of ML, whenever a model is not able to correlate input and output, the performance will be terrible. Underfitting is encountered when there are few training samples and it typically presents with a high rate of error for both training and testing. In contrast to this, overfitting occurs when the model cannot generalize on the task it was trained to perform due to overtraining, achieving a low error rate when training, but a high error rate when testing. In both of these cases, the model cannot find a good correlation between the input and output examples.

However it is not complicated to avoid underfitting of a model. A trivial way underfitting can be avoided is to increase the training samples. In the case this is not possible due to the small size of the dataset, techniques such as data augmentation (Section 2.4.6) in order to modify the currently existing data can be employed. Overfitting can also be avoided by providing more data, but with a higher diversity, or by performing dropout. That is, to explicitly disable perceptrons within the model in order to prevent a network to become more biased on training samples.

2.4.2 Common layers of CNN

This section describes some of the most common layers that are found in Artificial Neural Networks, which is absolutely mandatory before we present the different topologies of Convolutional Neural Networks. Usually, such operations are already implemented and ready-to-use in modern Machine Learning frameworks such as TensorFlow [1], PyTorch [25], Caffe [18] or Flux [17].

2.4.2.1 Pooling

Pooling is an operation that achieves subsampling (i.e. the reduction of data, by extracting only some parts of it) using a sliding window of a pre-defined size. Three popular variants of pooling are: max-pooling, min-pooling and average-pooling. Figure 2.7 illustrates the max-pooling operation: the sliding window is moving over the input data (a matrix structure in the case of Convolutional Neural Networks), extracting the maximum value from a sub-matrix with the width and height that corresponds to the window of the pooling operation. Since we are talking about a sliding window implementation, the number of positions a window moves over the input matrix is also called the “stride” size. Typically, this stride size is usually equal to the width or height of the window so that there are none overlaps or gaps.

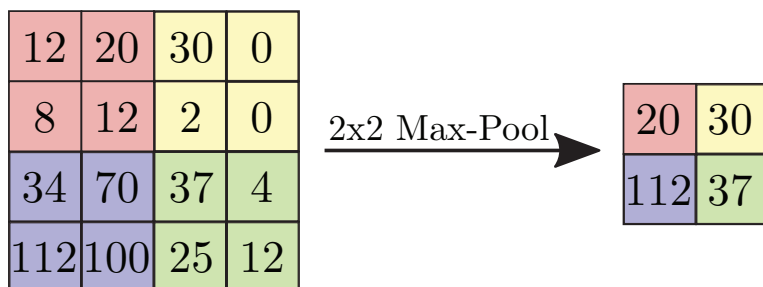


Figure 2.7: Max-pooling with a window size of 2x2 and a stride of 2.

This example should suffice for the pooling operation. It should be evident from the naming that the operations of min or average pooling extract the minimum, and respectively, the average of the sub-matrix, sharing the same working principle.

2.4.2.2 Convolution

The layer which give CNN their name, the convolution operation is the one in charge of learning what in the literature are called “feature maps” or “activation maps”. A visualisation of such feature maps can be seen in Figure 2.8. The features that are detected early on within the topology of a convolutional neural network are called “lower-level features” and are seen as simple lines, edges. Deeper in the network, feature maps become more complex, building on lower-level features. Those end up as the features that influence the decision proces of a model.

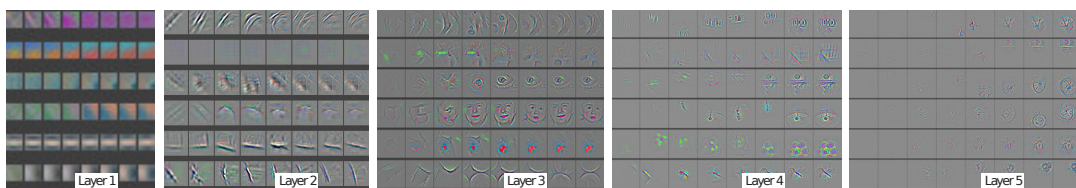


Figure 2.8: Feature maps learned after convolution layers [34]

2.4.2.3 Upsampling

The purpose of upsampling is to resample the data back to it’s initial sampling rate. The CNN architectures described in this chapter present two different methods of achieving upsampling. This operation is sometimes called “zero stuffing” due to the fact that missing values are replaced with zero-values¹¹ in order to perform the upsampling. Two main ways this process is performed is either through the reverse of convolution (deconvolution) or like in the case of SegNet, through reusing the indices from max pooling. Figure 2.9 illustrates the usage for both these techniques.

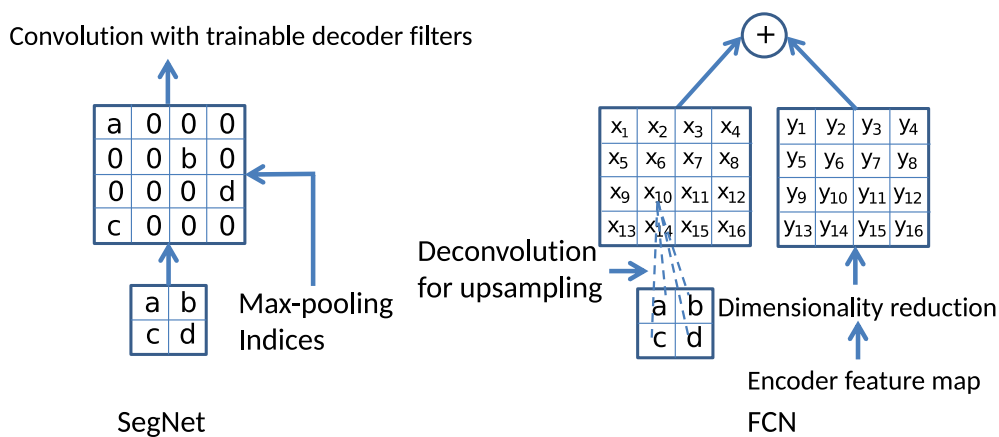


Figure 2.9: Max-pooling indices (left) [2] — deconvolution(right)

¹¹This can be also seen as interpolation.

2.4.2.4 Softmax

Softmax (or softargmax) is a layer which typically found at the end of an CNN. It normalises and converts a vector containing real numbers into a probability distribution with the number of probabilities equal to the number of elements in the vector. Due to the nature of softmax being the last layer in a network, it is usually also called the softmax classifier. Softmax takes the form of:

$$s(x_i) = \frac{e^{x_i}}{\sum_{j=1}^n e^{x_j}}$$

2.4.2.5 Activation Functions

Part of perceptrons (Figure 2.6) found in a typical ANN, activation functions help in deciding if a certain perceptron will take part further into the network (that is, it will propagate it's output to the next layer, hence called an "activated perceptron"). Activation functions can be either linear or nonlinear. It is not possible to use linear activation functions with CNN¹² due to the training algorithm's need to compute the derivate of such a linear function, therefore correlation to any input value will be lost, more details in Section 2.4.1. The current section showcases some of the widely used activation functions that are nonlinear and relevant to the present work.

Sigmoid

The Sigmoid (σ) function is a widely used activation function due to it's properties: it is differentiable, monotonic, it has a smooth gradient and the output values are bound to the interval $[0, 1]$. A major disadvantage of Sigmoid is that at the ends of the function it's values are not very influenced by the input value, hence their derivative will converge to 0, otherwise known as the "vanishing gradient" problem.

$$\sigma(x) = \frac{1}{1 + e^{-x}}$$

$$\sigma'(x) = \frac{e^{-x}}{(1 + e^{-x})^2}$$

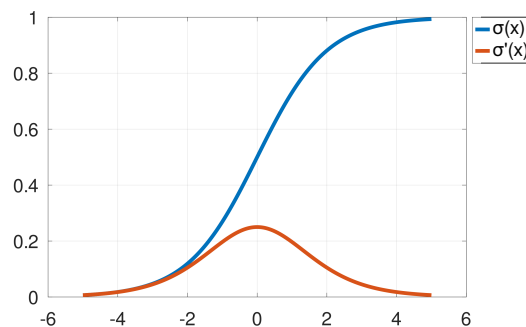


Figure 2.10: The Sigmoid function

Tanh

Tanh, or the hyperbolic tangent function is similar to the Sigmoid function. Output values are bound to the interval $[-1, 1]$ and the advantage over Sigmoid is that it has a steeper derivative, therefore the vanishing gradient problem does not appear.

¹²Linear activation functions can be used to solve linear regression tasks for example.

$$\tanh(x) = \frac{e^x - e^{-x}}{e^x + e^{-x}}$$

$$\tanh'(x) = 1 - \tanh(x)^2$$

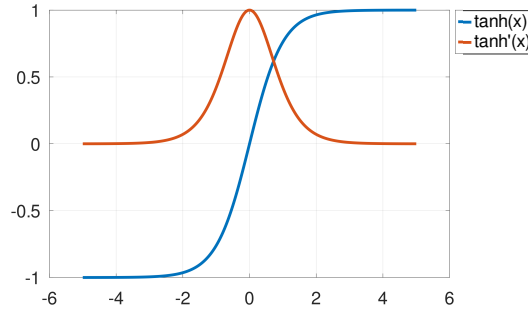


Figure 2.11: The Tanh function

ELU, ReLU and Leaky ReLU

Exponential Linear Unit (ELU) is an activation function that also solves the vanishing gradient problem. It is highly cost-efficient therefore it leads to improving the training time of a CNN. ELU also contains an α value which typically holds a small value (popular choices are between 0.1, 0.3).

$$ELU(x) = \begin{cases} \alpha(e^x - 1), & x < 0, \\ x, & x \geq 0, \end{cases}$$

$$ELU'(x) = \begin{cases} ELU(x) + \alpha, & x \leq 0, \\ 1, & x > 0, \end{cases}$$

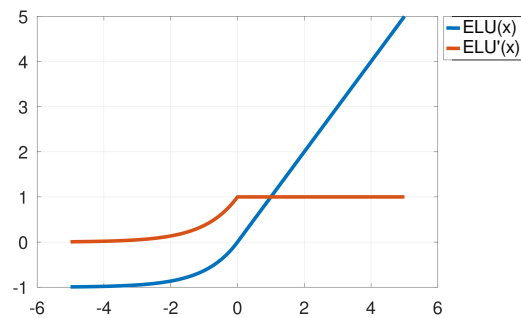


Figure 2.12: The ELU function

ReLU solves the vanishing gradient problem as well, but introduces a problem called the “dead ReLU” - the derivative of the ReLU function provides an explanation. It’s output is binary, we get either 0 or 1 values. But for values that are smaller than 0 the output will always be 0. And hence a significant number of perceptrons will not be activated, causing dropout (Section 2.4.1) in the network.

$$ReLU(x) = \max(0, x)$$

$$ReLU'(x) = \begin{cases} 0, & x \leq 0, \\ 1, & x > 0, \end{cases}$$

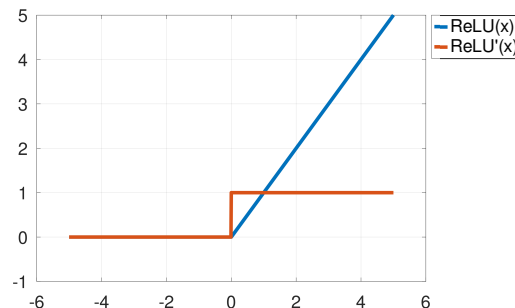


Figure 2.13: The ReLU function

The “dead ReLU” problem is fixed by Leaky ReLU. Because of the α value, output of Leaky ReLU cannot be 0, and is instead a small positive value in cases when the input value x is less than 0. It is also faster to compute than ELU due to not having to compute the exponential function.

$$LReLU(x) = \begin{cases} \alpha x, & x \leq 0, \\ x, & x > 0, \end{cases}$$

$$LReLU'(x) = \begin{cases} \alpha, & x \leq 0, \\ 1, & x > 0, \end{cases}$$

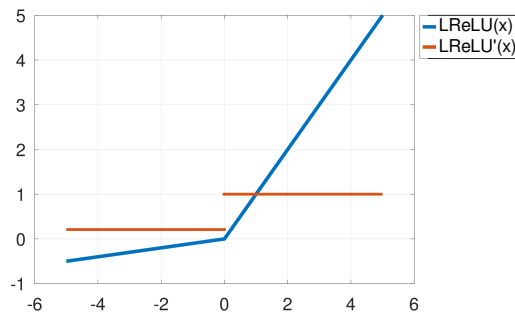


Figure 2.14: The LReLU function

2.4.3 Optimizers

Although backpropagation (Section 2.4.1) has already been briefly discussed, and mentions on how the algorithm helps with computing gradients, therefore providing with information on how to adapt weights in an ANN, an optimizer is responsible with actually changing various parameters within a network. Besides changing the weights the role of an optimizer is to also changes other parameters, such as the learning rate. The learning rate is a parameter that specifies the size of a step when searching for a local minimum of a loss function (this loss function is the same one described in Section 2.4.1).

2.4.3.1 Gradient Descent

Popular with solving tasks such as linear regression or classification, and with the fact that backpropagation also makes use of gradient descent. It is an optimization algorithm which computes how weights in the network should be changed in such a way as to minimize the value of a loss function so that it can reach a global minima.

Gradient descent has a few disadvantages: namely, that it could get stuck in a local minima and not reach to find a global one. Also, the optimizer modifies the weights only after computing gradients on the whole dataset, because of this convergence to the global minima can be inefficient in terms of both time and memory usage.

Stochastic Gradient Descent (SGD)

Stochastic Gradient Descent (SGD) is an improvement over simple gradient descent in that, parameters are updated at regular intervals, therefore requiring less time to converge to a global minima. The disadvantage is that SGD might continue to converge even after reaching a global minima due to constantly updating parameters.

2.4.3.2 Adam

Adam (or Adaptive Moment Estimation) is an optimizer that works with momentums (which are an heuristic for improving convergence in order to find a global minima). The advantage of Adam, since momentums are used is that the convergence is typically fast, but at a high computational cost.

2.4.4 Fully Convolutional Neural Networks

Fully Convolutional Neural Networks [23] (FCN) are different from typical CNN by not containing fully connected layers. The fully connecting layers are instead replaced by convolutions (Section 2.4.2.2) with a filter size equal to the size of input data. This conversion allows for networks which are trained for classifying images into outputting heatmaps (such is the example seen in Figure 2.15) of the features which determine the model into attributing a certain class to the input image.

In comparison to state of the art CNN topologies, the proposal of converting typical fully connected networks (this process is also called convolutionalization) FCN that were designed by [23] show an increase of accuracy performance of up to 20% compared to the same topologies which contain regular fully connected layers.

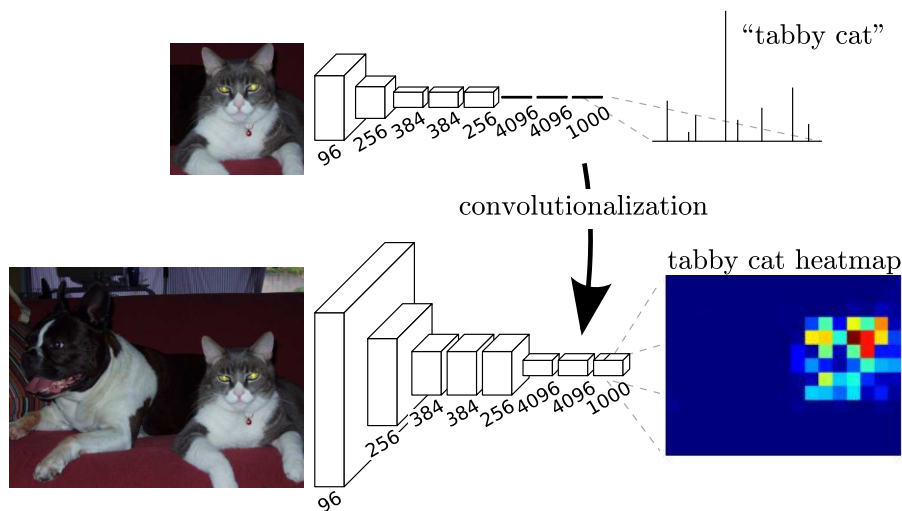


Figure 2.15: Fully convolutional network convolutionalization [23]

2.4.5 SegNet

SegNet [2] is a fully-convolutional (Section 2.4.4) Neural Network that was designed specifically with semantic segmentation in mind. The topology of this network is comprised of two parts: an encoder and a decoder. Based on VGG16 [28], the first 13 convolutional layers (which comprise the encoder part) of SegNet are identical: multiple convolution layers followed by batch normalization and ReLU activation and max-pooling with a 2x2 window and a stride of 2. Each layer in the encoder has a corresponding layer within the decoder where upsampling is performed.

According to [2], one of the incentives for developing SegNet is the ability to map low-resolution feature maps generated in the encoder part of the network with higher-resolution features (which are created with the help of upsampling) into the decoder of the network, therefore making the task of boundary localization easier. This approach is one that is proven beneficial for pixelwise semantic segmentation.

Each block in the encoder part of the network contains a convolution followed by batch normalization and a ReLU activation function later followed by max-pooling for downsampling data 2.16. Fully connected layers are removed in order to free memory to contain higher resolution feature maps. Additionally, using max-pooling indices instead of keeping the entire feature maps from encoding reduces memory when inferencing data compared to other approaches of FCN [2].

The architecture of SegNet is differentiated from other CNN based on how it handles the upsampling process. Namely, max-pooling indices are reused in order to resample the image to bigger dimensions (Section 2.4.2.3). It therefore eliminates the need of using deconvolutions (which how most networks learn to resample data).

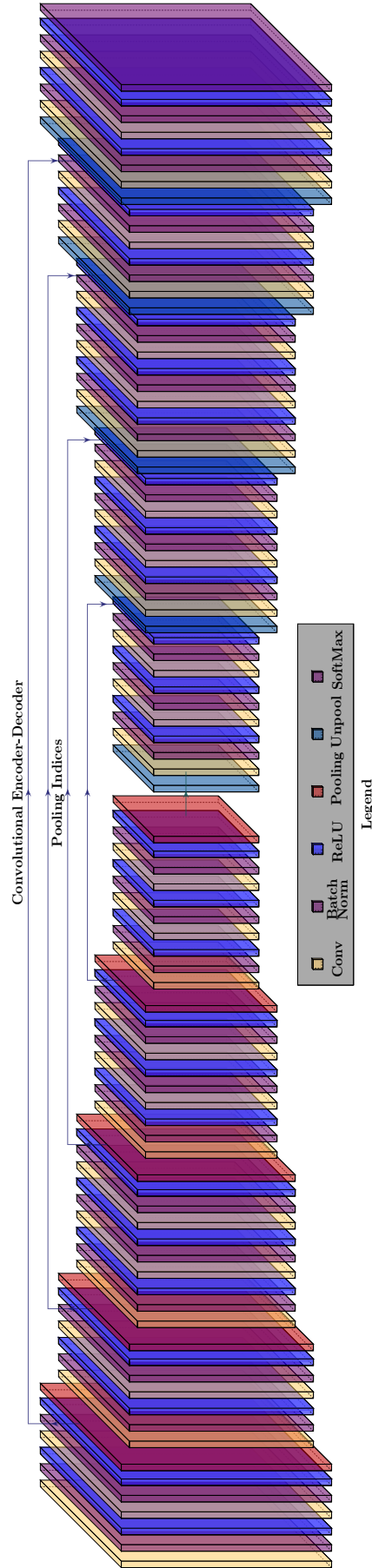


Figure 2.16: The SegNet architecture [2]

2.4.6 U-Net

U-Net [27] is another FCN model, which was created for semantic segmentation of biomedical images, specifically electron microscopy imagery. The lack of available datasets within this specific field has led to developing a CNN which is able to perform well on small datasets, while heavily relying upon augmentation techniques.

U-Net also uses an encoder-decoder topology, and is comprised of 32 convolution layers. The layers found in the U-Net architecture are similar to the ones in SegNet: 3x3 convolutions, followed by ReLU activation and max-pooling with a 2x2 window and stride size of 2. Every downsampling part in the encoder doubles the number of features found in the network. U-Net performs upsampling by deconvolution (Section 2.4.2.3) that reduces the number of feature channels in half. Feature maps from the corresponding layer in the encoder are cropped and concatenated to the ones found in the decoder, followed by 3x3 convolutions and ReLU. The network uses a 1x1 convolution at the end for mapping each output vector to a class 2.17. This 1x1 convolution can be usually replaced by the softmax function 2.4.2.4. The motivation for cropping and concatenating the feature maps is that of propagating information faster in the network.

U-Net was trained for solving semantic segmentation on electron microscopy images. Since the dataset was relatively small in samples, data augmentation techniques were used, such as: deformations, rotation and shifts. Additionally, U-Net has already been used with Remote Sensing data [9, 15, 33] yielding satisfactory results.

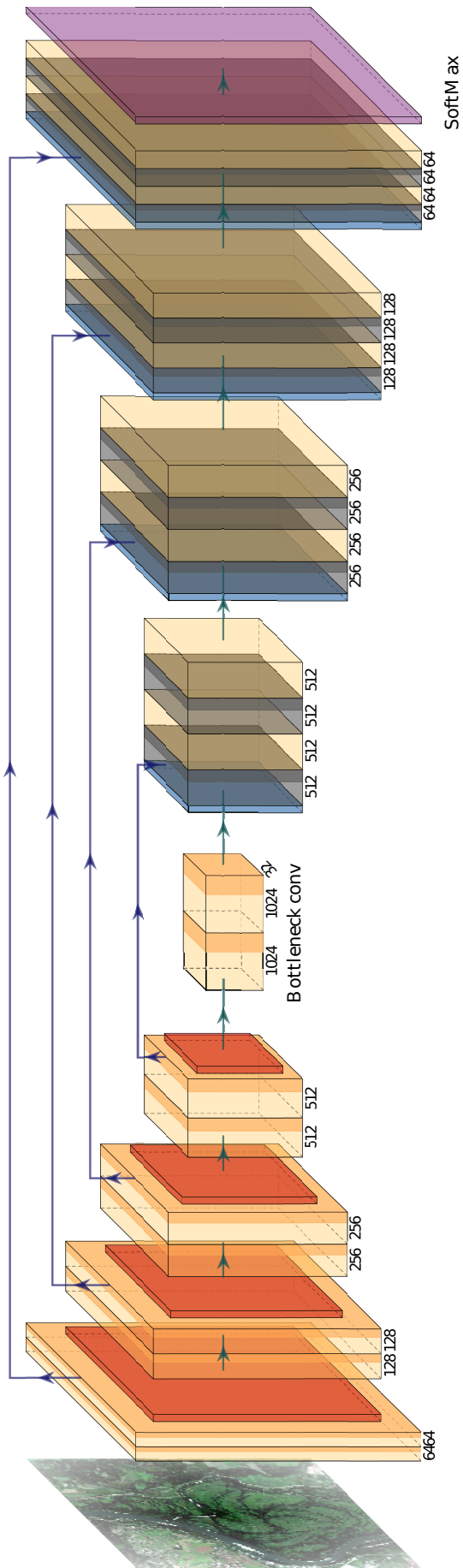


Figure 2.17: The U-Net architecture [27]

2.4.7 ResNet

ResNet [15] proposes a solution for creating models that are resistant to the problem of accuracy degrading over time. This problem usually occurs when using deep neural network topologies and has the effect of restricting the number of layers of a network as to not produce high error rates. The proposed method is the introduction of residual units (Figure 2.18) in the network. This approach has been verified by adapting deep neural networks and training on datasets such as ImageNet [10], CIFAR-10 [20] or MS-COCO [22]. Improvements over training time and overall model accuracy while using the aforementioned datasets have also been shown [15].

2.4.7.1 Residual Units

A residual unit (also known as a “skip connection”) is a shortcut between layers of an ANN. Adding skip connections helps with avoiding the vanishing gradient problem: when training the gradient produced by backpropagation for a given weight can become small, hence making weights stop updating their values. The proposal with ResNet [15] helps backpropagation propagate gradients through the skip connections more conveniently. Using residual units with U-Net and other topologies has been shown to reduce the number of parameters and training time [35].

Concatenating the output from previous layers is performed by using an identity mapping (Figure 2.18). In the case of a difference between dimensions of a layer that needs to be concatenated (due to having convolutions or pooling layers) either zero-stuffing or the use of 1x1 convolutions is employed. Figure 2.18 shows a residual unit compared to a typical convolution block found within a typical CNN.

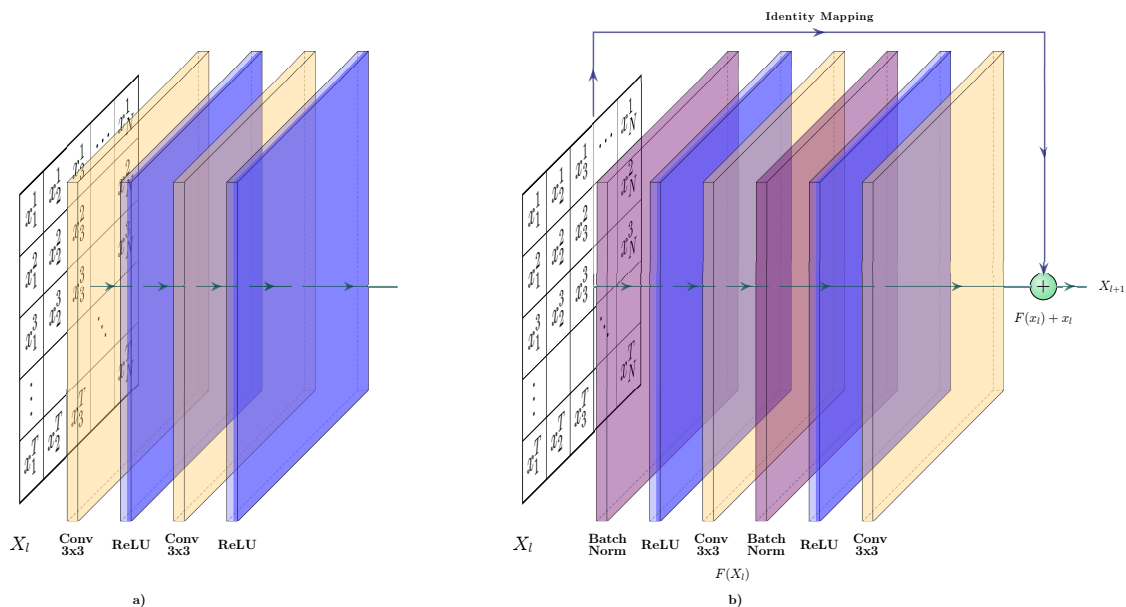


Figure 2.18: a) Simple convolution layers — b) Residual Unit [15]

2.5 Measuring the performance of models

There are numerous means of quantifying the performance yielded by a Machine Learning algorithm. This section is dedicated to showcasing some of those methods. Beforehand, we should introduce the notions of True Positives, True Negatives, False Positives and False Negatives. This is shown within Table 2.5, also called a “confusion matrix”. Varying from what a Machine Learning model predicts and what the actual class is¹³, the result is classified into one of these four categories.

	Predicted Positive	Predicted Negative
Actual Positive	True Positive	False Negative
Actual Negative	False Positive	True Negative

2.5.1 Accuracy: is it enough?

Accuracy is a very commonly used way of measuring how many samples a Machine Learning model can correctly predict out of the whole validation dataset.

$$accuracy = \frac{TN + TP}{TP + FP + TN + FN}$$

While accuracy can give us an insight of the number of samples a given model correctly predicts, there exists one problem: It might not be representative to the problem. This is the case when True Positives highly outnumber True Negatives or vice versa. In scenarios where, for example, a model would learn to perform the task classification, relying on accuracy only as an evaluation metric might be problematic, we could have a high accuracy rate (such as $\geq 90\%$), but what our model might be doing is actually classifying all the samples as the class corresponding to True Negatives. *In other words, if we have 10.000 True Positives, and 1.000 True Negatives samples, a model that would classify all the samples as True Positives, will have an accuracy of 91%, which does not sound bad at all, but our model will only be classifying one class.* Taking all of this into consideration, accuracy cannot be always relied upon as the only means of evaluating the performance of a model.

2.5.2 Precision & Recall

Given the problem discussed in the previous section regarding accuracy, there exist other metrics which can be used as an alternative to keep track of the performance yielded by a ML model, namely precision and recall. Precision is represented as:

$$precision = \frac{TP}{TP + FP}$$

From the above formula, we can understand that precision is used as a means of identifying how many of the samples our model classified as positive (TP + FP), are

¹³In Remote Sensing, the actual class is also called the “ground truth”.

indeed actual positives samples. *If a model correctly classifies 910 samples (either true or false positives) out of 1000 true positives, it's precision would be 91%.*

The recall metric, on the other hand tells us how many samples that are relevant (TP + FN) are classified appropriately by our model. *If a model classifies 940 samples (either true positives or false negatives) out of 1000 true positives or false negatives, it's recall is 94%.*

$$recall = \frac{TP}{TP + FN}$$

2.5.3 F-score / Sørensen-Dice coefficient

This metric is taking into consideration both precision and recall for measuring the accuracy of a ML model. The key difference between this metric and the simple accuracy shown previously, is that F-score is the weight added to both false negatives and false positives. Hence, larger numbers of true negatives will not have as big of an impact as in the case of simple accuracy. F-1 score is expressed as:

$$F_1 = 2 * \frac{precision * recall}{precision + recall}$$

The Sørensen-Dice coefficient (DSC) is a particular case of the F_1 score, when either one of precision or recall has a value of 0, and it can be written as:

$$DSC = \frac{2TP}{2TP + FP + FN}$$

2.5.4 IoU/Jaccard index & MIoU

MIoU or the Jaccard index is a metric used typically in measuring the performance of models for solving Computer Vision tasks.

$$Jaccard(X, Y) = \frac{|X \cap Y|}{|X \cup Y|}$$

Where the X and Y sets represent either bounding boxes, or segmentation masks for the ground truth (X), and predictions performed by the model (Y).

2.6 Multi-modal learning

Multi-modal learning [5] employs the principle that multiple different kinds of data from multiple sources are used in order to develop an automated model that is capable of performing on a given task. Similar to what a human experiences, that is receiving multiple information from different sources (through systems such as vision, auditory, olfactory, sensory). In the context of ML the nature of the data dictates how learning representations should be achieved.

One of the main challenges of multi-modal learning is that of correlating data (also known as alignment). In the case of Remote Sensing, alignment has to be done both temporal and spatial to assure relevance of the data from an holistic standpoint. Other multi-modal learning techniques encompass the correlation of text audio and/or images. When dealing with multiple sources that produce similar data (such as imagery that is represented as a matrix structure) there are multiple possibilities of achieving multi-modal training. Additionally, learning representations (Section 1.3) from data spanning multiple different sources increases the complexity of multi-modal learning. Data fusion is the ability to aggregate the information in such a way that one or multiple models are capable of yielding informed predictions.

Using multiple-input CNN topologies is a method of achieving multi-modal training. The working principle with multiple inputs is that data is fed to the network on separate input layers and is to be fused later into the topology. This process is usually performed by using typical operations of CNN (described in Section 2.4.2).

Ensemble learning [36] (otherwise known as “committee-based learning”) is another method multi-modal learning can be performed. The principle is to train separate models using data from separate sources and to use a consensus algorithm after predicting in order to reach a decision, taking into consideration the features learned by each model based on the data that was given.

In the current work, three different sources of data are aggregated in order to build a dataset designed for multi-modal learning (Section 3.4). Data gathered by the Sentinel-3 OLCI instrument is supposed to provide additional information to the Sentinel-2 MSI data. Additionally CLC data further enhances the available information, providing ground truth which necessary for performing supervised learning.

2.7 Introducing Hugin: Machine Learning using remote sensing data

Hugin¹⁴ is a ML framework specifically designed to work with multiple geospatial raster data formats. Currently built on top of the Keras¹⁵ library, it provides support for solving CV tasks such as classification, semantic segmentation or super-resolution and data fusion. It allows for training CNN models with data acquired by Remote Sensing techniques (e.g. those discussed within Section 2.2).

Hugin is highly configurable (Appendix C) based on YAML¹⁶ files for explicitly controlling both the training and testing processes. Included in these configuration files are data sources (with support for local or cloud based object storage such as Amazon S3 Buckets¹⁷). Hugin can correlate multiple data sources, load models from paths to custom built or existing Keras model builders, change parameters to these models such as optimizers (Section 2.4.3) and their respective parameters, loss functions, performance monitoring metrics (Section 2.5). Control over introducing Keras callbacks that aid the training process is also included, some examples such as as stopping training a model if a specified treshold of change in a given metric is not met after a converging for a while or heuristics for reducing the learning rate.

When dealing with datasets with particularly large images, Hugin can also perform image tiling automatically by an implemented sliding window algorithm which can be configured by using the YAML files. It also provides aid when data is too large to fit into memory when training, therefore loading data in predefined batches.

Checkpointing is a useful feature that has been added within Hugin for saving the weights of a model either at specified intervals, or saving only the weights of the model which achieves the best overall performance in terms of a monitored metric.

Predictions are also configurable with Hugin, with support for both unimodal and ensemble predictions. The output of predictions is controlled by using either a specialised raster writer such as RasterIO¹⁸ or by wrapping custom format exporters. Similar to training configuration, predictions can also be specified which model loaders, and data sources to use.

¹⁴<https://pypi.org/project/hugin/>

¹⁵<https://keras.io/>

¹⁶<https://yaml.org/>

¹⁷<https://aws.amazon.com/s3/>

¹⁸<https://rasterio.readthedocs.io/en/latest/>

Chapter 3

Semantic segmentation of vegetation in Remote Sensing imagery: an approach based on Machine Learning

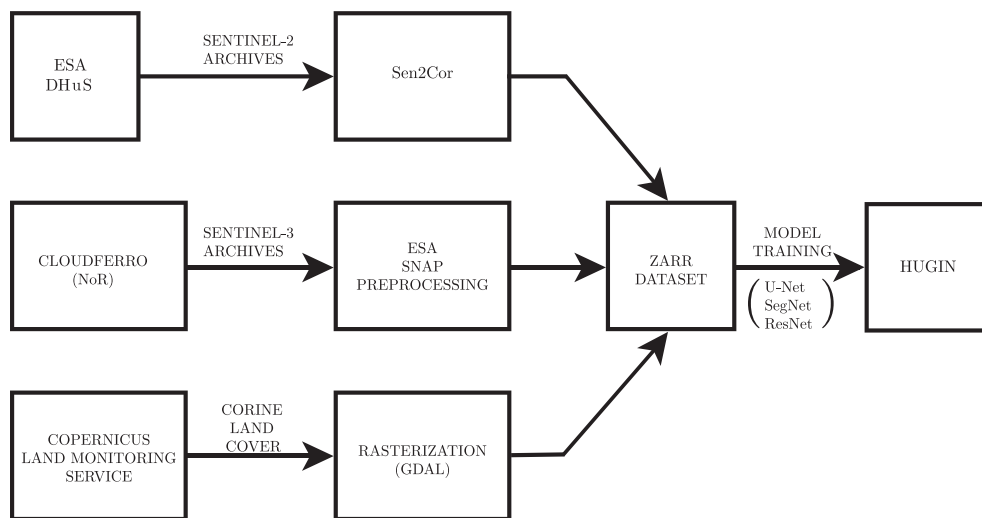


Figure 3.1: The processing pipeline

Figure 3.1 illustrates the pipeline that was used for solving the problem of semantic segmentation of vegetation classes in the current approach. Three different data sources are used: ESA DHuS, the CloudFerro¹ cloud provider, and the Copernicus Land Monitoring Service². Data from these sources was each later preprocessed in a specific way, and stored using the hierarchical zarr³ data storage format. This data was later used in order to train three different configurations of CNN (which are described in Sections 2.4.5, 2.4.6, 2.4.7) with the help of the Hugin ML framework (Section 2.7). Specifics regarding the training process are described within Section 3.5, and the results of applying these methods are presented in Chapter 4.

¹<https://cloudferro.com/en/>

²<https://land.copernicus.eu/>

³<https://zarr.readthedocs.io/en/stable/>

3.1 ESA DHuS as a data source

Satellite imagery gathered by the Copernicus programme is distributed through the ESA Ground Segment⁴. Data is free to use and to redistribute and is available within any of the multiple Data Hub Software (DHuS). DHuS nodes for distributing data that are synchronized with official ESA instances can be operated by entrusted⁵ entities of the Copernicus programme, those instances are called collaborative nodes.

3.1.1 Extracting data from DHuS

Each DHuS instance provides with two methods for searching Sentinel products: a web interface, and an OpenSearch⁶ API. The API includes means of filtering data based on sensing period, Sentinel mission, product type, processing level, percentage of cloud coverage or missing data. Support for filtering data by geographical location is also available, provided the usage of a markup language specifically designed for representing geometrical objects that are georeferenced: Well Known Text (WKT).

Since the web interface does not support for downloading data in bulk, we want to programatically extract Sentinel archives through the available OpenSearch API (an example of usage can be found in Appendix A). The Sentinelsat⁷ project provides an implementation of an DHuS OpenSearch client that is easily configurable for searching and retrieving archives from all the Sentinel missions found within DHuS.

Sentinelsat was used for filtering Sentinel-2 archives that we're acquired on the territory of Romania for the year of 2018 in order to keep relevance with the land cover classes in the CLC inventory. The filtered archives we're then retrieved and processed using Sen2cor for extraction of cloud masks and cloud shadow masks 3.3.3.

3.1.2 Current limitations of DHuS and alternatives

Within the DHuS services a rolling plan was introduced⁸ in which older archives are placed inside of a long-term archive (LTA). The data is still available for retrieval by users within 24 hours per archive, on a by request basis that is limited to one archive per day. Although ESA sustains a great ammount of data, the rate at which data is being produced and the infrastructure requirements for serving archives have grown recently in such a manner that storing older archives in LTA has become mandatory.

Additionally with the growth of data, ESA has developed the EO NoR initiative, supporting research and development with the help of subcontracting partners which provide RS data and processing services in the cloud. To work around the LTA issue, the current approach was sponsored for fulfilling a NoR request with the scope of retrieving and processing Sentinel-3 OLCI archives in order to complete the dataset. The retrieval and processing of Sentinel-3 OLCI archives for the year of 2018 has been accomplished in the CloudFerro cloud, which besides cloud computing capabilities it also provides a collection of unarchived Copernicus mission imagery.

⁴esa.int/Applications/Observing_the_Earth/Copernicus/Ground_Segment_overview

⁵By the European Commission (EC)

⁶<https://scihub.copernicus.eu/userguide/OpenSearchAPI>

⁷<https://github.com/sentinelsat/sentinelsat>

⁸<https://scihub.copernicus.eu/userguide/LongTermArchive>

3.2 Sentinel-2 and Sentinel-3 archives

Sentinel-2

Currently with two satellites in orbit, Sentinel-2A and Sentinel-2B which together have a revisit time of 5 days (meaning they pass through the same geographic location to acquire data at an interval of 5 days). The Sentinel-2 products provide MSI data at three different spatial resolutions (60m, 30m, and 10m) covering a wide spectrum. MSI reflectance data is important for providing spectral signatures of different objects which can be used for classifying different objects. The contents of a Sentinel-2 MSI archive are listed in Appendix A. Sentinel-2 products for 2017 from the AOI are included in the proposed dataset (described fully in Section 3.4).

Sentinel-3 OLCI

The OLCI instrument on board of the two Sentinel-3 (Sentinel-3A and Sentinel-3B) satellites provides with additional information about land coverage at a revisit time of two days. This information is useful for enhancing Sentinel-2 MSI data and for performing multi-modal learning (Section 2.6). Contents of the Sentinel-3 OLCI archives (which are listed within Appendix A) include as previously mentioned (in Section 2.1), reflectance data for all of the 21 bands of the OLCI instrument, tie geometries, high resolution georeferencing, meteorology data, removed pixels informations and quality control flags.

3.3 Data preprocessing

Before constructing the dataset and performing multi-modal learning, data from all the aforementioned sources has to be preprocessed. In the context of the current work, this includes reprojection of Sentinel-3 archives so we can correlate them to Sentinel-2 and CLC data. Since CLC is distributed in vectorial format, it needs to be rasterized at the same spatial resolution as the Sentinel-2 data in order for alignment of input and output data to be possible.

3.3.1 Reprojecting Sentinel-3 archives using ESA GPT

Sentinel-3 OLCI archives include reflectance data for each band in separate files. The georeferencing is also stored in a separate file. For relevance, we want to include georeferencing information and store all the bands in a single master file. Additionally, bands information in a Sentinel-3 archive are provided in a NetCDF-4⁹ format, for uniformity and similarity to the other data, we want to rewrite the data into GeoTIFF¹⁰ format. The ESA SNAP (Sentinel Application Platform) provides multiple toolkits for interacting with data acquired by the Copernicus programme. Processing graphs (example in Appendix B) can be described using XML format and executed with the help of the Graph Processing Tool (GPT).

⁹<https://www.loc.gov/preservation/digital/formats/fdd/fdd000332.shtml>

¹⁰<https://www.loc.gov/preservation/digital/formats/fdd/fdd000279.shtml>

3.3.2 Corine Land Cover rasterization

Corine Land Cover CLC is distributed in vector format (there exist a raster which is distributed as well, but it was rasterized at 100 meter resolution). To achieve a finer granularity, the vector CLC data which is distributed under the proprietary ESRI OpenFileGDB format is rasterized using the GDAL¹¹ *gdal_rasterize* tool at a resolution of 10m. The output of this process is a single GeoTIFF file containing all the information from initial the CLC vector. Since our AOI is the entire territory of Romania, the output raster was cropped to a bounding box which is expressed as an WKT polygon and passed to *gdal_rasterize* that delimits the whole AOI.

3.3.3 Cloud masks - Sen2Cor

Sen2cor [24] is a processor for Sentinel-2 Level-2A BOA reflectance products. The processor is present within the SNAP toolbox for Sentinel-2, and it can perform classification (SCL) of 11 classes (with two important classes which are belonging to cloud and cloud shadows - medium and high cloud probabilities). It can be used to also perform atmospheric corrections in Sentinel-2 archives. Sen2cor was used in the context of the current work for generating cloud masks, in order for regions of imagery that are occluded (Section 2.3.1) by clouds to be ignored by the model and not taken in as samples of a class present in the CLC inventory.

3.3.4 Tiling and mosaicking

In order to obtain a finer granularity (in terms of selecting data from a specific geographic location, but also being memory efficient) making data easier to handle, in the case of RS data it is common to divide rasters into smaller chunks called tiles. This was the approach taken with the proposed dataset. Sentinel-2 MSI data was chunked into tile sizes of 256x256 with 4 dimensions (one for each band) for the bands with 10m resolution, 6 dimensions for bands at 20m and 3 for 60m. Sentinel-3 OLCI data was chunked in 9x9 tiles with 21 dimensions, since all the bands have the same spatial resolution of 300m.

For visualisation of scenes or for retrieving or computing global information in a particular area of interest, scenes are assembled based on their georeferencing into a mosaic. Several technologies including virtual rasters supported by GDAL can compose an aggregate of multiple rasters.

3.4 Constructing a multi-modal dataset

All the processing steps of the pipeline illustrated in Figure 3.1 for the data spanning three different sources have been described. Having as preprocessed output rasters for both Sentinel-2 MSI and Sentinel-3 OLCI stored in GeoTIFF format, data is tiled and added into a hierarchical data storage format, namely the zarr format.

¹¹<https://gdal.org/>

3.4.1 Zarr as a data storage format

Zarr is a hierarchical data format which is similar to HDF¹². It has support for storing chunked and compressed (using the `blosc`¹³ algorithm by default, but data can also be compressed with the `zlib`, `bz2` and `lzma` algorithms) multi-dimensional arrays spanning multiple different `numpy`¹⁴ data types. Since zarr is a hierarchical data storage format, it has support for creation of groups and arrays within groups.

The proposed structure for storing the Sentinel archives and the CLC inventory presented within the current work under zarr format is illustrated in Figure 3.2. It was designed in such a way to enable further enhancements and addition of data.

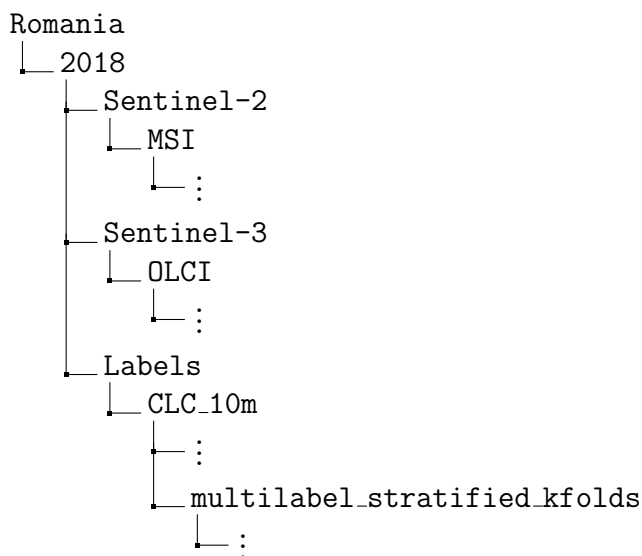


Figure 3.2: Directory tree for the zarr structure of the proposed dataset.

Figure 3.3 illustrates the array containing Sentinel-2 MSI 10m bands data for 51 weeks of the year 2018. It has a total size of 1.67TB, spanning on a width of 215 tiles and a height of 291 tiles (this width and height cover the whole AOI). Each tile has a size of 256x256 pixels and 4 channels (Red, Green, Blue and Near Infrared).

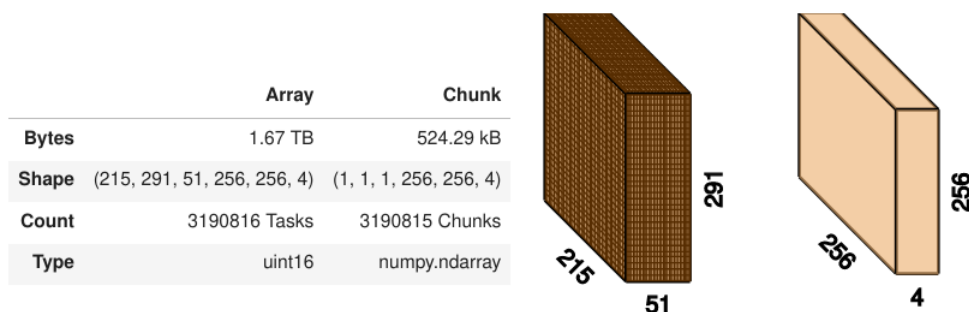


Figure 3.3: Sentinel-2 10m resolution data array for 51 weeks of year 2018.

¹²<https://portal.hdfgroup.org/display/HDF5/HDF5>

¹³<https://github.com/Blosc/c-blosc>

¹⁴<https://numpy.org/>

3.4.2 Splitting the dataset: Stratified K-folds

Simple methods for splitting the dataset into training and testing subsets, such as the `sklearn.model_selection.train_test_split`¹⁵ implemented in the scikit-learn library perform shuffling and splitting of the dataset in two sets, based on user defined proportions, a popular choice is using 80% for training and 20% for testing.

In order to avoid overfitting (described in Section 2.4.1) of any models we wish to train, technique was utilized for cross validation. K-fold cross validation gives information about how a model will be able to perform on samples it has not seen.

K-fold is an algorithm for splitting the dataset into subgroups of equal size for training and validation of models, which makes better use of the samples within a dataset by keeping each subgroup statistically representative of the entire dataset. The working principle of the K-fold algorithm are shown within Algorithm 1.

Algorithm 1: K-fold algorithm

Data: Input: $K > 1$; ▷ Number of groups
Data: Input: Θ ; ▷ Set of hyperparameters
Data: Input: D ; ▷ Initial dataset containing input and output data
Data: Input: M ; ▷ Trainable model
 $score = 0$;
partition D into K randomly equal size subsets $F_1 \dots F_K$;
foreach $\theta \in \Theta$ **do**
 for $i = 1$ to K **do**
 Use F_i as a validation dataset and the remaining folds for training;
 Fit data to model M using hyperparameter configuration θ ;
 Compute training error e of model M with for the holdout fold F_i ;
 end
 $score += \frac{e}{K}$;
end
return $score$

As illustrated in Algorithm 1 in the implementation of the K-fold algorithm, each subset K_i is used at least once for validation. This means that each sample in the dataset will be used once for validation and $K - 1$ times for training the model M .

There exist different techniques for choosing the value of K : Picking a value that would make sure that each validation and training set is large enough to be statistically representative for the entire dataset. $K = 10$ is a popular choice in the ML community. $K = n$ where n is the size of the dataset (this is called “leave-one-out cross validation”) will validate on one sample and use the rest folds for training.

Stratified cross validation with the k-fold algorithm is typically used when dealing with multiple labels (multilabel stratified k-fold). It ensures that when the dataset is split into subsets, each subset besides having the property of being equal to the other $K - 1$ sets, they will contain approximately the same number of samples of each class. Using the stratified variation of k-fold therefore preserves class ratio.

¹⁵<https://scikit-learn.org>

3.5 Training Convolutional Neural Networks with Hugin

The CNN architectures presented within Sections 2.4.5, 2.4.6 and 2.4.7 were used in order to train models on the task of semantic segmentation using 17 vegetation related classes of the proposed multi-modal dataset (Section 3.4).

In terms of configurations, each model was trained with the Adam optimizer 2.4.3.2 using categorical cross-entropy as a loss function. The metrics used for monitoring model performance are MIoU (Section 2.5.4), precision and recall (Section 2.5.2).

Categorical cross-entropy (which is Softmax + cross-entropy) was chosen as a loss function since our goal is to perform semantic segmentation for multiple classes of vegetation. The Adam optimizer was chosen to provide faster convergence, since training time grows significantly with the number of classes involved.

Keras callbacks such as early stopping and reducing of the learning rate when loss value on the validation dataset reaches a plateau were used in order to achieve better performance of the models. Checkpointing implemented in 2.7 was used to save only the weights for the epochs which achieved the best performance.

In order for the experiments to be deterministic in nature, we have configured Hugin to use random seeds for all the model and dataset initialization methods.

Training was performed on the proposed dataset that was split by using the Stratified K-folds algorithm (Section 3.4.2). The folds were created previous to the training process and stored in a separate group in the zarr format (Section 3.4).

The different model configurations were trained using data ranging from the weeks 14-40 of the year 2018 (from April to September) with the reasoning being that of having the most samples containing vegetation in different states.

Samples of YAML configuration files for Hugin can be found within Appendix C.

Chapter 4

Experiments

The current chapter presents results following training multiple CNN configurations (of topologies discussed in Sections 2.4.5, 2.4.6, 2.4.7) using the dataset proposed in Section 3.4 split using the K-folds 3.4.2 algorithm. The models were trained for semantic segmentation of vegetation using classes included in the CLC inventory.

Table 4.1 shows the performance of the trained models for the testing dataset. While adding a significant time overhead in order to converge, we can notice that SegNet does not yield satisfactory results being in fact, the worst overall model.

Although there exist a high number of training samples in the weeks that were selected for training (April to September) which include a small overall cloud cover percentage, and U-Net is a model that is designed to perform on small datasets, it has given the best performance overall, taking into account the MIoU metric.

Model	accuracy	precision	recall	MIoU
U-Net	0.772349	0.918345	0.500243	0.602314
U-Net	0.682321	0.921134	0.499213	0.553526
SegNet	0.425534	0.218452	0.323334	0.243481
ResNet	0.525591	0.748259	0.402512	0.288468
ResNet	0.588212	0.748592	0.448209	0.523451

Table 4.1: Performance metrics of trained models.

The training time for both U-Net and ResNet was almost half of the convergence time of SegNet, while yielding better performance using the same configuration (the Adam optimizer and Categorical cross-entropy as a loss function) with the same initialization parameters and the same inference of data.

Illustrated in Figure 4.1 are segmentation masks from U-Net and ResNet (both models for each network). Visually, we can notice that both trained topologies are able to produce segmentation masks, although with problems: some regions include sparse segmentation masks even if vegetation is still visible. For further correction of these masks postprocessing techniques in order to fill the sparse masks can be employed in order for the segmentation to be more complete. This can be performed using methods that include nearest-neighbor sampling or expansion of the masks.

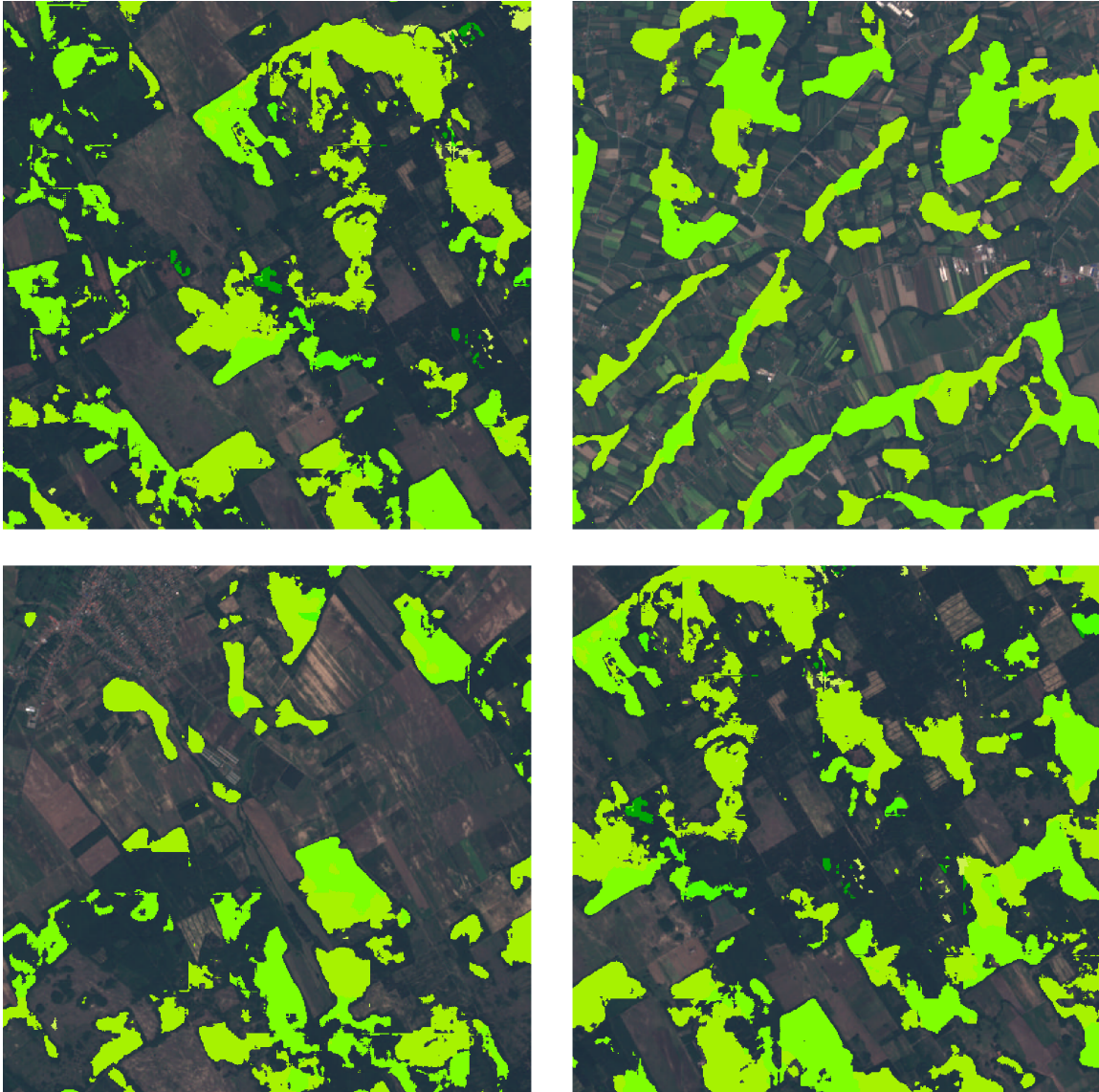


Figure 4.1: Output segmentation masks from the trained models U-Net(left) and ResNet (right)

Chapter 5

Conclusions

Summary

The current work has shown inner workings of Artificial Intelligence techniques based on Convolutional Neural Networks. Specifics of Remote Sensing and ways of processing data were also presented. We have highlighted a couple of existing datasets containing Remote Sensing data such as BigEarthNet (Section 2.2.2), SpaceNet (Section 2.2.1), Corine Land Cover (Section 2.2.3), MODIS Land Cover (Section 2.2.4) and LUCAS (Section 2.2.5). Specifics on building and training Machine Learning models such as common layers found in Convolutional Neural Networks (Section 2.4.2), activation functions for activation of perceptrons (Section 2.4.2.5), optimization methods (Section 2.4.3) and also topologies of commonly used Fully Convolutional Networks (Sections 2.4.5, 2.4.6, 2.4.7). Metrics for analyzing the performance of ML models are presented in 2.5. Problems that often arise when dealing with Computer Vision tasks were discussed in Section 2.3.1 but also ways of mitigating such problems. Techniques for performing Multi-modal learning are presented within Section 2.6.

A proposal for creating a new, multi-modal and spatio-temporal dataset that is relevant in the current context, providing data that is useful for solving the task of semantic segmentation for land cover/land use. With the aggregation of Sentinel-2 MSI and Sentinel-3 OLCI imagery, using Corine Land Cover CLC for ground truth information. The value added by this dataset is validated by showing how the task of semantic segmentation of vegetation can be solved with Convolutional Neural Networks by learning vegetation features from the proposed dataset.

Contributions

Given the current context of research in the fields of Remote Sensing and Machine Learning, the present work provides two important contributions: First, the creation of a new multi-modal and spatio-temporal dataset containing land cover information, paired with Sentinel-2 MSI and Sentinel-3 OLCI data. Second, the validation of the dataset by providing information regarding performance of models trained to solve semantic segmentation of vegetation by using the proposed dataset.

Open problems

Although the results of experimenting with models trained for semantic segmentation of vegetation shown in Chapter 4 provide some important results taking into account visual confirmation as proof of work as well, there are still open problems that interfere with the development of automated techniques based on Machine Learning.

Occlusion is one of the main problems that arise when dealing with Remote Sensing imagery, particularly when RGB data is used. Even if cloud formations can be identified by using processors such as Sen2cor (Section 3.3.3), they appear very frequently in Remote Sensing data. This unfortunately means that the number of samples we can reliably take into account when training Machine Learning models on such data is significantly reduced. More so, by observation we noticed that cloud formations appear more often during spring and autumn, therefore interfering with samples from these seasons, having to remove them from the training of models.

Future work

Further enhancements for the proposed dataset include the addition of Sentinel-1 SAR data for providing another modality of learning. Another benefit could come from adding other land cover inventories such as MODIS land cover and LUCAS, but this also increases the complexity of translation and alignment of data while also adding a significant processing overhead. CLC was chosen due to the granularity and multitude of land coverage classes it offers. Correlating Sentinel data with other inventories in the dataset could be proven as a benefit, but this implies in some cases the reduction of land cover classes since MODIS and LUCAS provide less in terms of classification schemes.

Additionally, including other cloud masks (Section 3.3.3) generated by the MAJA¹ and FMask² algorithms can further help with selecting relevant samples from the dataset which are not occluded by cloud formations.

¹<https://labo.obs-mip.fr/multitemp/maccs-how-it-works/>

²<https://github.com/GERSL/Fmask>

Bibliography

- [1] ABADI, M., AGARWAL, A., BARHAM, P., BREVDO, E., CHEN, Z., CITRO, C., CORRADO, G. S., DAVIS, A., DEAN, J., DEVIN, M., GHEMAWAT, S., GOODFELLOW, I., HARP, A., IRVING, G., ISARD, M., JIA, Y., JOZEFOWICZ, R., KAISER, L., KUDLUR, M., LEVENBERG, J., MANÉ, D., MONGA, R., MOORE, S., MURRAY, D., OLAH, C., SCHUSTER, M., SHLENS, J., STEINER, B., SUTSKEVER, I., TALWAR, K., TUCKER, P., VANHOUCHE, V., VASUDEVAN, V., VIÉGAS, F., VINYALS, O., WARDEN, P., WATTENBERG, M., WICKE, M., YU, Y., AND ZHENG, X. TensorFlow: Large-scale machine learning on heterogeneous systems, 2015. Software available from tensorflow.org.
- [2] BADRINARAYANAN, V., KENDALL, A., AND CIPOLLA, R. Segnet: A deep convolutional encoder-decoder architecture for image segmentation. *arXiv preprint arXiv:1511.00561* (2015).
- [3] BAETENS, L., DESJARDINS, C., AND HAGOLLE, O. Validation of copernicus sentinel-2 cloud masks obtained from maja, sen2cor, and fmask processors using reference cloud masks generated with a supervised active learning procedure. *Remote Sensing* 11, 4 (2019), 433.
- [4] BALLIN, M., BARCAROLI, G., MASSELLI, M., SCARNÓ, M., ET AL. Re-design sample for land use/cover area frame survey (lucas): 2018 edition.
- [5] BALTRUŠAITIS, T., AHUJA, C., AND MORENCY, L.-P. Multimodal machine learning: A survey and taxonomy. *IEEE transactions on pattern analysis and machine intelligence* 41, 2 (2018), 423–443.
- [6] BENEDIKTSSON, J. A., PESARESI, M., AND AMASON, K. Classification and feature extraction for remote sensing images from urban areas based on morphological transformations. *IEEE Transactions on Geoscience and Remote Sensing* 41, 9 (2003), 1940–1949.
- [7] BOSSARD, M., FERANEC, J., OTAHEL, J., ET AL. Corine land cover technical guide: Addendum 2000.
- [8] BROWN, T., MANE, D., ROY, A., ABADI, M., AND GILMER, J. Adversarial patch.
- [9] BUSLAEV, A., SEFERBEKOV, S., IGLOVIKOV, V., AND SHVETS, A. Fully convolutional network for automatic road extraction from satellite imagery. *CoRR*, *abs/1806.05182* (2018).

- [10] DENG, J., DONG, W., SOCHER, R., LI, L.-J., LI, K., AND FEI-FEI, L. Imagenet: A large-scale hierarchical image database. In *2009 IEEE conference on computer vision and pattern recognition* (2009), Ieee, pp. 248–255.
- [11] DUAN, P., WANG, Y., AND YIN, P. Remote sensing applications in monitoring of protected areas: A bibliometric analysis. *Remote Sensing* 12, 5 (2020), 772.
- [12] FERANEC, J., HAZEU, G., KOSZTRA, B., AND ARNOLD, S. Corine land cover nomenclature. In *European Landscape Dynamics*. CRC Press, 2016, pp. 47–56.
- [13] FRIEDL, M. A., SULLA-MENASHE, D., TAN, B., SCHNEIDER, A., RAMANKUTTY, N., SIBLEY, A., AND HUANG, X. Modis collection 5 global land cover: Algorithm refinements and characterization of new datasets. *Remote sensing of Environment* 114, 1 (2010), 168–182.
- [14] GOODFELLOW, I., BENGIO, Y., AND COURVILLE, A. *Deep Learning*. MIT Press, 2016. <http://www.deeplearningbook.org>.
- [15] HE, K., ZHANG, X., REN, S., AND SUN, J. Deep residual learning for image recognition. In *Proceedings of the IEEE conference on computer vision and pattern recognition* (2016), pp. 770–778.
- [16] HELBER, P., BISCHKE, B., DENGEL, A., AND BORTH, D. Eurosat: A novel dataset and deep learning benchmark for land use and land cover classification. *IEEE Journal of Selected Topics in Applied Earth Observations and Remote Sensing* 12, 7 (2019), 2217–2226.
- [17] INNES, M. Flux: Elegant machine learning with julia. *Journal of Open Source Software* 3, 25 (2018), 602.
- [18] JIA, Y., SHELFHAMER, E., DONAHUE, J., KARAYEV, S., LONG, J., GIRSHICK, R., GUADARRAMA, S., AND DARRELL, T. Caffe: Convolutional architecture for fast feature embedding. In *Proceedings of the 22nd ACM international conference on Multimedia* (2014), pp. 675–678.
- [19] KARPATY, A., AND JOHNSON, J. Cs231n convolutional neural networks for visual recognition-transfer learning. <https://cs231n.github.io/>.
- [20] KRIZHEVSKY, A., HINTON, G., ET AL. Learning multiple layers of features from tiny images.
- [21] LECUN, Y., BOSER, B., DENKER, J. S., HENDERSON, D., HOWARD, R. E., HUBBARD, W., AND JACKEL, L. D. Backpropagation applied to handwritten zip code recognition. *Neural Comput.* 1, 4 (Dec. 1989), 541–551.
- [22] LIN, T.-Y., MAIRE, M., BELONGIE, S., HAYS, J., PERONA, P., RAMANAN, D., DOLLÁR, P., AND ZITNICK, C. L. Microsoft coco: Common objects in context. In *European conference on computer vision* (2014), Springer, pp. 740–755.

- [23] LONG, J., SHELHAMER, E., AND DARRELL, T. Fully convolutional networks for semantic segmentation. In *Proceedings of the IEEE conference on computer vision and pattern recognition* (2015), pp. 3431–3440.
- [24] MAIN-KNORN, M., PFLUG, B., LOUIS, J., DEBAECKER, V., MÜLLER-WILM, U., AND GASCON, F. Sen2cor for sentinel-2. In *Image and Signal Processing for Remote Sensing XXIII* (2017), vol. 10427, International Society for Optics and Photonics, p. 1042704.
- [25] PASZKE, A., GROSS, S., MASSA, F., LERER, A., BRADBURY, J., CHANAN, G., KILLEEN, T., LIN, Z., GIMELSHEIN, N., ANTIGA, L., ET AL. Pytorch: An imperative style, high-performance deep learning library. *arXiv preprint arXiv:1912.01703* (2019).
- [26] PLAZA, A., MARTÍNEZ, P., PLAZA, J., AND PÉREZ, R. Dimensionality reduction and classification of hyperspectral image data using sequences of extended morphological transformations. *IEEE Transactions on Geoscience and remote sensing* 43, 3 (2005), 466–479.
- [27] RONNEBERGER, O., FISCHER, P., AND BROX, T. U-net: Convolutional networks for biomedical image segmentation. *International Conference on Medical image computing and computer-assisted intervention* (2015), 234–241.
- [28] SIMONYAN, K., AND ZISSERMAN, A. Very deep convolutional networks for large-scale image recognition. *arXiv preprint arXiv:1409.1556* (2014).
- [29] SULLA-MENASHE, D., AND FRIEDL, M. Mcd12q1 modis/terra+ aqua land cover type yearly l3 global 500m sin grid v006. *NASA EOSDIS Land Processes DAAC: Sioux Falls, SD, USA* (2019).
- [30] SUMBUL, G., CHARFUELAN, M., DEMIR, B., AND MARKL, V. Bigearth-net: A large-scale benchmark archive for remote sensing image understanding. In *IGARSS 2019-2019 IEEE International Geoscience and Remote Sensing Symposium* (2019), IEEE, pp. 5901–5904.
- [31] SZEGEDY, C., LIU, W., JIA, Y., Sermanet, P., REED, S., ANGUELOV, D., ERHAN, D., VANHOUCHE, V., AND RABINOVICH, A. Going deeper with convolutions. In *Proceedings of the IEEE conference on computer vision and pattern recognition* (2015), pp. 1–9.
- [32] TSOELENG, L. T., ODINDI, J., AND MHANGARA, P. A comparison of two morphological techniques in the classification of urban land cover. *Remote Sensing* 12, 7 (2020), 1089.
- [33] VAN ETTEN, A., LINDENBAUM, D., AND BACASTOW, T. M. Spacenet: A remote sensing dataset and challenge series. *arXiv preprint arXiv:1807.01232* (2018).
- [34] ZEILER, M. D., AND FERGUS, R. Visualizing and understanding convolutional networks. In *European conference on computer vision* (2014), Springer, pp. 818–833.
- [35] ZHANG, Z., LIU, Q., AND WANG, Y. Road extraction by deep residual u-net. *IEEE Geoscience and Remote Sensing Letters* 15, 5 (2018), 749–753.

- [36] ZHOU, Z.-H. Ensemble learning. In *Machine Learning*. Springer, 2021, pp. 181–210.

Appendix A

Remote Sensing

Passive and active Remote Sensing

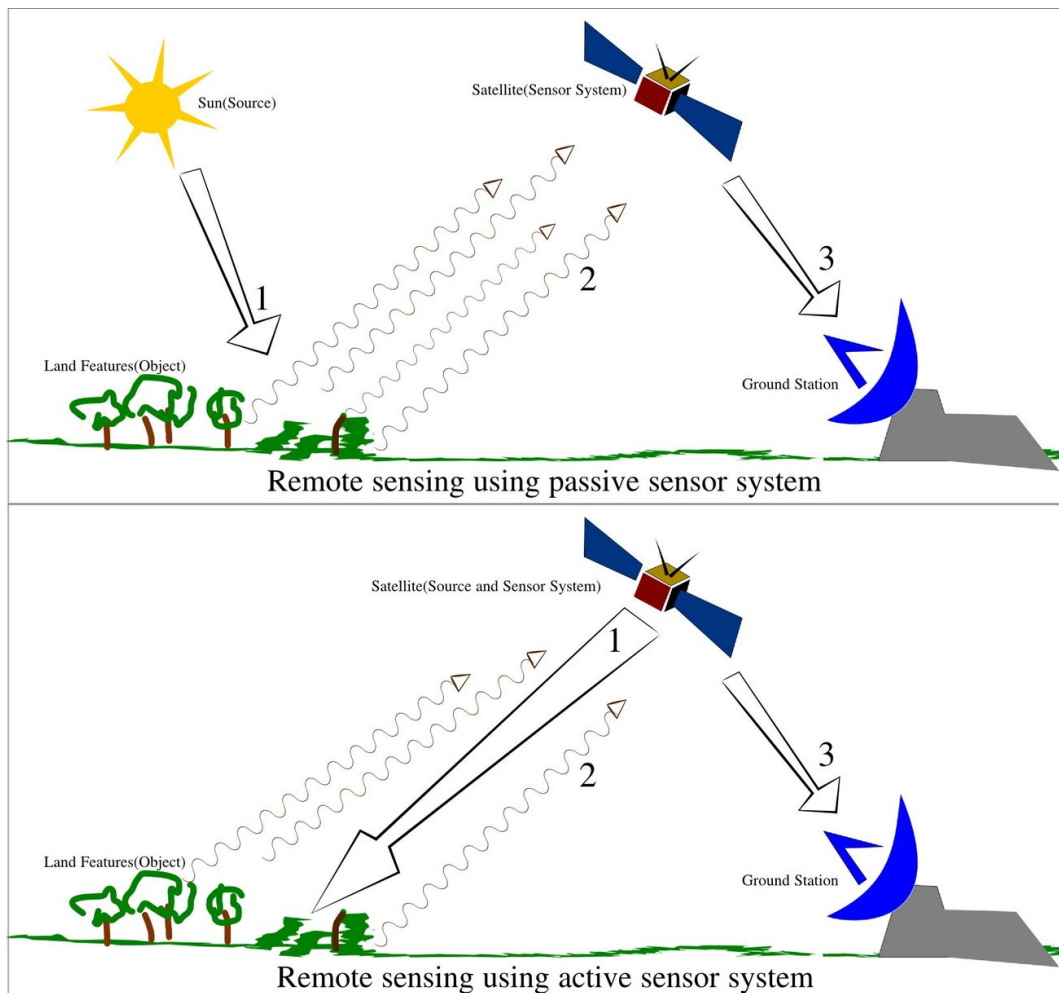


Figure A.1: Difference the between active and passive Remote Sensing
Arkarjun, CC BY-SA 3.0 (<https://creativecommons.org/licenses/by-sa/3.0/>), via Wikimedia Commons
https://commons.wikimedia.org/wiki/File:Remote_Sensing_Illustration.jpg

Data regarding land coverage of Romania

Figure A.2 showcases the breakdown of land coverage into the Corine Land Cover (CLC) Level-1 classes for the territory of Romania for the year 2018. We can notice that vegetation occupies 91.5% (agricultural areas & forest and semi-natural areas) of the land cover from the AOI of the current work.

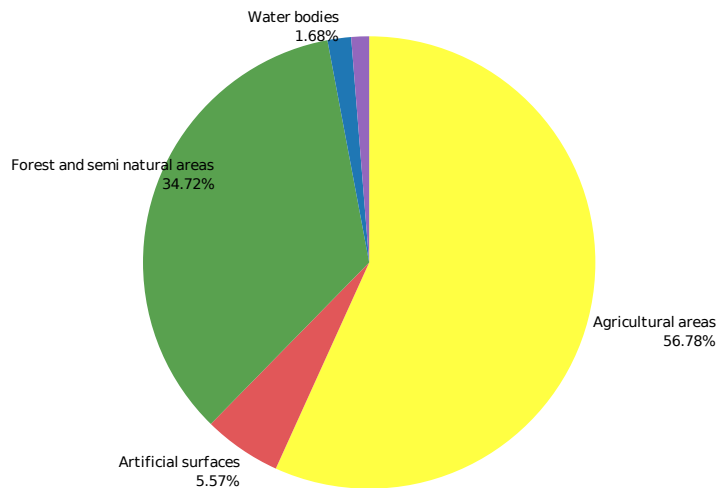


Figure A.2: Land cover in Romania as of 2018
Plot created with <https://land.copernicus.eu/dashboards/clc-clcc-2000-2018>

Using the DHuS OpenSearch API

The OpenSearch API provided by DHuS instances can be queried for retrieving data using a cURL GET request:

```
$curl --request GET 'https://scihub.copernicus.eu/dhus/api/stub/products
?filter=(
beginPosition:[2018-06-01T00:00:00.000Z TO 2018-09-01T23:59:59.999Z] AND
endPosition:[2018-06-01T00:00:00.000Z TO 2018-09-01T23:59:59.999Z]) AND
((platformname:Sentinel-3 AND filename:S3B_* AND
producttype:OL_1_EFR__ AND instrumentshortname:OLCI))
AND footprint: Intersects
(POLYGON((16.58910503349143 43.400842665330345,
26.95841113834191 43.400842665330345,
26.95841113834191 49.09541206485471,
16.58910503349143 49.09541206485471,
16.58910503349143 43.400842665330345)))
&offset=0&limit=25&sortedby=ingestiondate&order=desc'
```

Contents of an Sentinel-3 OLCI archive

geo_coordinates.nc
instrument_data.nc
0a01_radiance.nc
0a02_radiance.nc
0a03_radiance.nc
0a04_radiance.nc
0a05_radiance.nc
0a06_radiance.nc
0a07_radiance.nc
0a08_radiance.nc
0a09_radiance.nc
0a10_radiance.nc
0a11_radiance.nc
0a12_radiance.nc
0a13_radiance.nc
0a14_radiance.nc
0a15_radiance.nc
0a16_radiance.nc
0a17_radiance.nc
0a18_radiance.nc
0a19_radiance.nc
0a20_radiance.nc
0a21_radiance.nc
qualityFlags.nc
removed_pixels.nc
S3A_OL_1_EFR___20181231T081701_20181231...LN1_0_NT_002-ql.jpg
tie_geo_coordinates.nc
tie_geometries.nc
tie_meteo.nc
time_coordinates.nc
xfdumanifest.xml

Contents of an Sentinel-2 MSI archive

```

AUX_DATA
├── DATASTRIP
│   ├── DS_CREO_20210115T195324_S20180831T133222
│   │   ├── MTD_DS.xml
│   │   └── QI_DATA
└── GRANULE
    ├── L2A_T22LGL_A016666_20180831T133222
    │   ├── AUX_DATA
    │   │   └── AUX_ECMWFT
    │   ├── IMG_DATA
    │   │   ├── R10m
    │   │   │   ├── T22LGL_20180831T133221_AOT_10m.jp2
    │   │   │   ├── T22LGL_20180831T133221_B02_10m.jp2
    │   │   │   ├── ...
    │   │   │   ├── T22LGL_20180831T133221_TCI_10m.jp2
    │   │   │   └── T22LGL_20180831T133221_WVP_10m.jp2
    │   │   ├── R20m
    │   │   │   ├── T22LGL_20180831T133221_AOT_20m.jp2
    │   │   │   ├── T22LGL_20180831T133221_B02_20m.jp2
    │   │   │   ├── ...
    │   │   │   ├── T22LGL_20180831T133221_B8A_20m.jp2
    │   │   │   ├── T22LGL_20180831T133221_SCL_20m.jp2
    │   │   │   ├── T22LGL_20180831T133221_TCI_20m.jp2
    │   │   │   └── T22LGL_20180831T133221_WVP_20m.jp2
    │   │   └── R60m
    │   │       ├── T22LGL_20180831T133221_AOT_60m.jp2
    │   │       ├── ...
    │   │       ├── T22LGL_20180831T133221_B8A_60m.jp2
    │   │       ├── T22LGL_20180831T133221_SCL_60m.jp2
    │   │       ├── T22LGL_20180831T133221_TCI_60m.jp2
    │   │       └── T22LGL_20180831T133221_WVP_60m.jp2
    │   └── MTD_TL.xml
    │       └── QI_DATA
    │           ├── FORMAT_CORRECTNESS.xml
    │           ├── GENERAL_QUALITY.xml
    │           ├── GEOMETRIC_QUALITY.xml
    │           ├── MSK_CLDPRB_20m.jp2
    │           ├── MSK_CLDPRB_60m.jp2
    │           ├── MSK_CLOUDS_B00.gml
    │           ├── MSK_DEFECT_B01.gml
    │           ├── MSK_DEFECT_B02.gml
    │           ├── MSK_DEFECT_B03.gml
    │           ├── ...
    │           ├── MSK_DETFOO_B01.gml
    │           └── MSK_DETFOO_B02.gml

```


- MSK_DETF00_B03.gml
- ...
- MSK_NODATA_B01.gml
- MSK_NODATA_B02.gml
- MSK_NODATA_B03.gml
- ...
- MSK_SATURA_B01.gml
- MSK_SATURA_B02.gml
- MSK_SATURA_B03.gml
- ...
- MSK_SNWPRB_20m.jp2
- MSK_SNWPRB_60m.jp2
- MSK_TECQUA_B01.gml
- MSK_TECQUA_B02.gml
- MSK_TECQUA_B03.gml
- ...
- SENSOR_QUALITY.xml
- T22LGL_20180831T133221_PVI.jp2
- INSPIRE.xml
- manifest.safe
- MTD_MSIL2A.xml
- rep_info
 - S2_PDI_Level-2A_Datastrip_Metadata.xsd
 - S2_PDI_Level-2A_Tile_Metadata.xsd
 - S2_User_Product_Level-2A_Metadata.xsd
- S2A_MSIL2A_20180831T133221_N0213_R081_T22LGL_20210115T195322-ql.jpg

Appendix B

Sentinel-3 GPT preprocessing

Using the Graph Processing Tool (GPT) from ESA's SNAP, we define an XML configuration of a pipeline that reprojects the data in an EPSG:4326 projection, extracting the bands we desire, placing them into a single GeoTIFF file:

```
1 <graph id="Graph">
2   <version>1.0</version>
3   <node id="Reproject">
4     <operator>Reproject</operator>
5     <sources>
6       <sourceProduct>${sourceProduct}</sourceProduct>
7     </sources>
8     <parameters>
9       <crs>EPSG:4326</crs>
10      <resampling>Nearest</resampling>
11      <noDataValue>NaN</noDataValue>
12      <includeTiePointGrids>true</includeTiePointGrids>
13    </parameters>
14  </node>
15  <node id="BandsExtract">
16    <operator>BandsExtractorOp</operator>
17    <sources>
18      <sourceProduct refid="Reproject"/>
19    </sources>
20    <parameters>
21      <sourceBandNames>
22        0a01_radiance,0a02_radiance, ..., 0a21_radiance
23      </sourceBandNames>
24      <sourceMaskNames></sourceMaskNames>
25    </parameters>
26  </node>
27  <node id="Write_1">
28    <operator>Write</operator>
29    <sources>
30      <sourceProduct refid="BandsExtract"/>
31    </sources>
32    <parameters>
33      <file>${targetFile}</file>
34      <formatName>GeoTIFF-BigTIFF</formatName>
35    </parameters>
36  </node>
37 </graph>
```

Appendix C

Hugin configuration examples

```
1 configuration:
2   model_path: "s3://sagegroup-data/alex/models/{name}"
3   name: "unet6-clc-vegetation"
4   workspace: "/home/alex/models/{name}"
5
6 data_source: !!python/object/apply:hugin.io.ZarrArrayLoader
7   kwds:
8     source: "s3://sagegroup-data/zarr/romania/2018/"
9     flat: False
10    slice_timestamps: [14, 32]
11    inputs:
12      input_1:
13        component: "Sentinel-2/10m"
14      input_2:
15        component: "Sentinel-2/presence_mask"
16    targets:
17      output_1:
18        component: "labels/clc/clc_10m"
19    split_train_index_array: "labels/clc/samples/clc_10m/classes"
20    split_test_index_array: "labels/clc/samples/clc_10m/classes"
21    randomise: True
22    random_seed: 42
23
24 trainer: !!python/object/apply:hugin.engine.scene.ArrayModelTrainer
25   kwds:
26     name: unet_clc_vegetation_2018
27     model: !!python/object/apply:hugin.engine.keras.KerasModel
28     kwds:
29       name: keras_model
30       model_builder: hugin.models.unet.unet3:unet
31       swap_axes: True
32       random_seed: 42
33       model_builder_options:
34         output_channels: 8
35       model_path: "/data/bid/storage0/sage-storage/homes/sage/alex/models/{name}"
36       batch_size: 1
37       epochs: 100
38       metrics:
39         - !!python/object/apply:hugin.tools.utils.MultilabelMeanIOU
40           kwds: { name: 'MeanIOU', num_classes: 8 }
41       loss: categorical_crossentropy
```

```
42     checkpoint:
43         monitor: val_loss
44     enable_multi_gpu: False
45     num_gpus: 1
46     use_multiprocessing: False
47     workers: 12
48     max_queue_size: 6
49     optimizer: !!python/object/apply:tensorflow.keras.optimizers.Adam
50     kwds:
51         lr: !!float 0.001 # 0.0001
52         beta_1: !!float 0.9
53         beta_2: !!float 0.999
54         epsilon: !!float 1e-7
55     callbacks:
56     - !!python/object/apply:tensorflow.keras.callbacks.EarlyStopping
57         kwds:
58             monitor: 'val_loss'
59             min_delta: 0.001
60             patience: 20
61             verbose: 1
62             mode: 'auto'
63             baseline: null
64             restore_best_weights: False
65     - !!python/object/apply:tensorflow.keras.callbacks.ReduceLROnPlateau
66         kwds:
67             monitor: 'val_loss'
68             patience: 5
69             factor: !!float 0.2
```

Appendix D

Additional experiments results

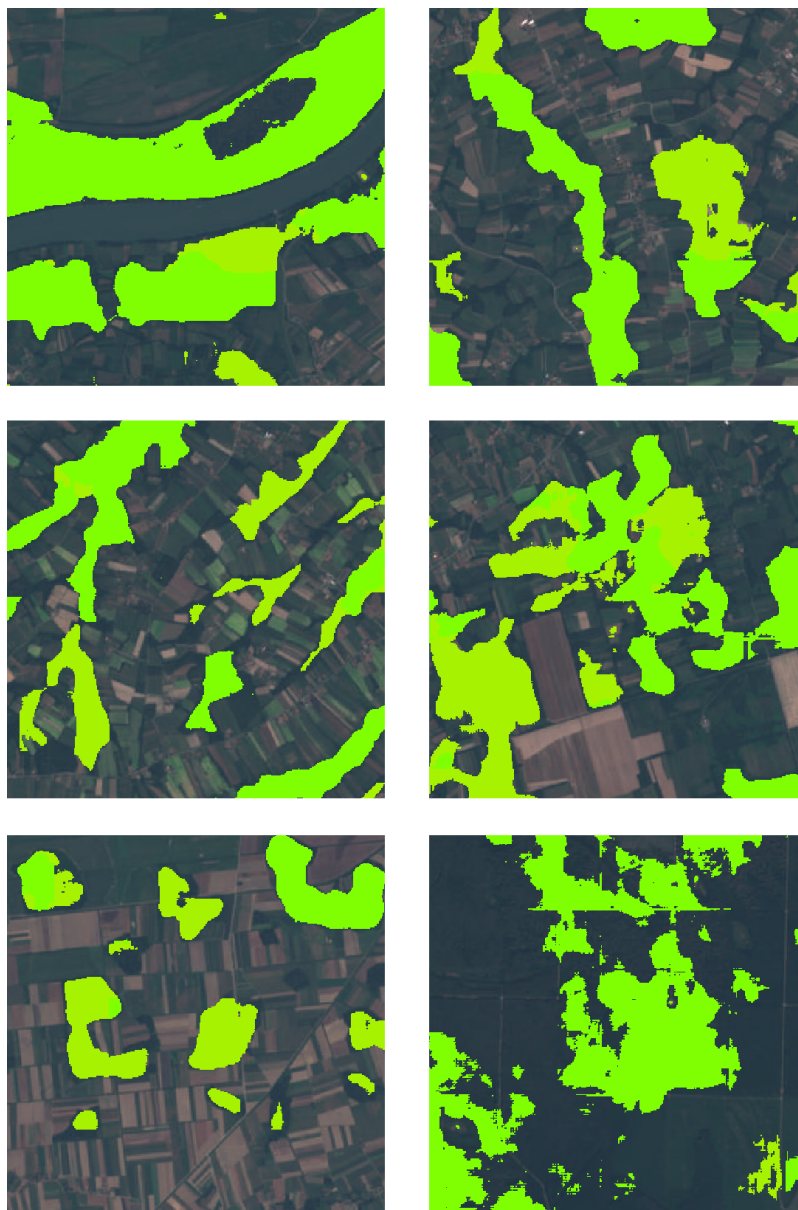


Figure D.1: Segmentation maps from the U-Net and ResNet models.